Popular extreme sea level metrics can better communicate impacts

D.J. Rasmussen, Scott Kulp, Robert E. Kopp, Michael Oppenheimer, and Benjamin H. Strauss

Draft: August 24, 2021

Abstract Estimates of changes in the frequency or height of contemporary extreme sea levels (ESLs) under various climate change scenarios are often used by climate and sea level scientists to help communicate the physical basis for societal concern regarding sea-level rise. Changes in ESLs (i.e., the hazard) are often represented using various metrics and indicators that, when anchored to salient impacts on human systems and the natural environment, provide useful information to policy makers, stakeholders, and the general public. While changes in hazards are often anchored to impacts at local scales, aggregate global summary metrics generally lack the context of local exposure and vulnerability that facilitates translating hazards into impacts. Contextualizing changes in hazards is also needed when communicating the timing of when projected ESL frequencies cross critical thresholds, such as the year in which ESLs higher than the design height benchmark of protective infrastructure (e.g., the 100-yr water level) are expected to occur within the lifetime of that infrastructure. We present specific examples demonstrating the need for such contextualization using a simple flood exposure model, local sea-level rise projections, and population exposure estimates for 414 global cities. We suggest regional and global climate assessment reports integrate global, regional, and local perspectives on coastal risk to address hazard, vulnerability and exposure simultaneously.

1 Introduction

Extreme sea levels (ESLs) are short-lived (hours to days), exceptionally high local sea-surface heights, usually resulting from coastal storms, waves, or astronomical tides (Gregory et al, 2019). Observational studies show that contemporary ESLs are occurring with increasing frequency, largely as a result of rising local mean sea level due to global warming and other non-climatic local factors (e.g., ground subsidence; Sweet and Park, 2014; Dahl et al, 2017; Menéndez and Woodworth, 2010). Future changes in ESL frequency pose significant hazards to coastal communities, natural resources, and ecosystem services (Oppenheimer et al, 2019). Potentially deadly and costly floods can occur in unprepared areas if ESLs overtop natural (e.g., dunes, cliffs) or engineered protection structures (e.g., seawalls, bulkheads, levees). Communicating the risks of changing ESLs can build trust between experts and the public, raise awareness, enhance the understanding of risks, develop agreement about policy options, and motivate pre-emptive risk reduction measures (Rowan, 1991). In the case of coastal flooding, the latter includes purchasing flood insurance, elevating assets (e.g.,

D.J. Rasmussen
Princeton School of Public & International Affairs, Princeton University, Princeton, NJ, USA. E-mail: dj.rasmussen@princeton.edu

Scott Kulp and Benjamin H. Strauss
Climate Central, Princeton, NJ, USA

Robert E. Kopp
Department of Earth & Planetary Sciences, Rutgers Energy Institute, and Institute of Earth, Ocean, & Atmospheric Sciences, Rutgers University, New Brunswick, NJ, USA.

Michael Oppenheimer
Department of Geosciences and Princeton School of Public & International Affairs, Princeton University, Princeton, NJ, USA.

regrading or placing homes on stilts), planning long-term land use strategies, such as coastal retreat, and implementing hard protection (Oppenheimer et al, 2019; Rasmussen et al, 2020, 2021).

Climate and sea level scientists have developed various metrics and indicators to describe changes in the frequency of contemporary ESLs under various climate change scenarios (Hunter, 2012; Buchanan et al, 2017; Rasmussen et al, 2018; Frederikse et al, 2020; Vitousek et al, 2017; Taherkhani et al, 2020; Church et al, 2013; Howard and Palmer, 2020; Feng et al, 2018; Fox-Kemper et al, 2021). For example, ESL amplification factors (AFs; also called "factors of increase" or "multiplication factors") denote the change in the expected frequency of a given contemporary ESL under a given climate change scenario. ESL frequency AFs denote the expected relative increase in the number of threshold exceedances per year, the threshold usually being an arbitrary return level measured at a tide gauge. In addition to appearing in the primary peer-reviewed literature, ESL AFs have been used to communicate changes in ESLs to policy makers, stakeholders, and the general public in climate assessment reports, such as the Intergovernmental Panel on Climate Change's (IPCC) Sixth Assessment Report (AR6; Fox-Kemper et al, 2021), Special Report on Global Warming of 1.5 °C (SR1.5; Hoegh-Guldberg et al, 2018), Special Report on Oceans and the Cryosphere (SROCC; Oppenheimer et al, 2019), and the Fourth U.S. National Climate Assessment Report (U.S. NCA; Sweet et al, 2017).

Despite their wide-spread use, ESL AFs have a few notable limitations in communicating impacts at regional and global scales. First, ESL AFs only consider the hazard component of risk, that being the physical heights of water surfaces. They do not consider corresponding levels of exposure (e.g., population, property value, or natural resources), nor do they consider vulnerability. Some human settlements may be protected to a level above the height of the ESL in question (i.e., no flood occurs), or there may exist little to no exposure at or below the ESL height (i.e., a flood occurs, but there is no meaningful impact). Locally, ESLs AFs can be anchored to salient impacts on human systems and the natural environment, such as the frequency of overtopping existing flood defenses, roadway flooding, sewer or drainage back-ups, and the depth of the historically experienced King Tide event (e.g., Sweet et al, 2018). Without this local information, changes in ESL hazard provide no human or ecological context. Second, ESL AFs and other indicators (e.g., changes in return levels) are generally presented for arbitrary years (e.g., 2050, 2100), which does not provide information about the likelihood of when impacts could cross critical thresholds for a particular location. Third, ESL AFs often highlight single return periods (e.g., the 1-in-100-year ESL, or an event comparable to a specific historic occurrence), potentially neglecting return periods that may be more salient for evaluation of risk for a given location.

In the remainder of this essay, we discuss each of these limitations and show that they can be overcome at regional or global scales. In light of the latter, we provide recommendations for communicating changes in ESLs in future climate assessment reports. Throughout, we use a simple flood exposure model to illustrate our points. Our methods are described in the Appendix.

2 Contextualize extreme sea level frequency changes at global scales

Unlike local analyses, regional and global-scale assessments often do not anchor ESL AFs to impacts, leading to uninformative summary statements that provide little insight for risk communication. For example, the IPCC presently makes summary statements about ESL hazards at the global scale that are based on arbitrary water levels and are not anchored to specific events. This de-contextualizes changes in ESLs. More specifically, in Chapter 4 of the SROCC it is stated, "...extreme sea level event estimates as presented in [Section 4.2.3.4.1], clearly show that as a consequence of sea level rise, events which are currently rare (e.g., with an average return period of 100 years), will occur annually or more frequently at most available locations for RCP8.5 by the end of the century (high confidence)" (Oppenheimer et al, 2019), and also in Chapter 9 of AR6, "Due to relative sea level rise, extreme sea level events that occurred once per century in the recent past are projected to occur at least annually at more than half of all tide gauge locations by 2100 (high confidence)" (Fox-Kemper et al, 2021). While these statements may be true for the hazard, it provides no information about the event exposure or consequence, perhaps leaving the reader to infer that 1) such currently rare events will be destructive wherever they occur or 2) more frequent historical recurrence times are of little importance (e.g., tidal flooding that compounds over time, Moftakhari et al, 2017).

For some locations, the contemporary 100-yr ESL is impactful, but for other locations it is not. Here we illustrate "impact" as the percent of the 2010 total population of a city that is inundated. For example, by

2070, the frequency of the contemporary 100-yr ESL for San Juan (Puerto Rico) is projected to increase from 0.01 events/yr to > 31 events/yr, on average, under a scenario in which global average surface air temperature (GSAT) stabilizes at +2 °C above preindustrial levels (an ESL AF of ∼3100; Table 1; Fig. 1A). However, < 0.1% of the 2010 total population of San Juan, Puerto Rico (<1,000 out of 1.8 million people) is exposed to the contemporary 100-yr ESL (Fig. 1B), as estimated using return levels from the local tide gauge and the bathtub flood modeling approach (see Appendix for details). The associated expected increase in population exposure from projected ESLs is ∼40% but is still < 1,000 people in absolute terms. Overall, an increase in the frequency of the contemporary 100-yr ESL will inundate relatively few San Juan residents (assuming constant population). On the other hand, ∼2.3% of the total population of the Norfolk/Hampton Roads region of Virginia, USA (∼16,000 out of 695,000 people) is exposed to the contemporary 100-yr ESL, which is expected to occur more than three times per decade by 2070 (ESL AF of ∼32; Table 1, Fig. 1D). Despite the ESL frequency AF for Norfolk being almost 100 times less than San Juan, the associated increase in population exposure is ∼3 times larger (Fig. 1C,D; Table 1).

To illustrate this discrepancy globally, we consider both the expected change in the frequency of the contemporary 100-yr ESL at tide gauges matched to 414 global cities (ESL frequency AF; Fig. 2A) and the expected relative change in number of people in each city exposed to the contemporary 100-yr ESL (the "population exposure AF"; Fig. 2B). We then group the cities by geographic region to look for regional patterns (Fig. 2C). Relationships between these metrics vary by city, in part due to differences in projected relative sea level change (RSLC; Gregory et al, 2019) and the shape of both the ESL return curves and the population versus elevation profiles (e.g., Fig. 1B,D). Across all regions, there is no strong relationship between changes in the frequency of the 100-yr ESL and changes in population exposure to the 100-yr event. Thus, ESL frequency AFs are, by themselves, poor proxies for impact, shown here in terms of total population exposure. Rather than a summary statement that considers only physical changes in ESL frequencies, one could—using this analysis—construct a statement that considers aggregate population exposure changes, "projected 2070 RSLC under an end-of-century +2 °C GSAT stabilization scenario (relative to pre-industrial) is expected to at least double the 2010 population exposed to the 100-yr ESL for 25% of the 414 coastal cities assessed, growing to 37% under an end-of-century +5 °C GSAT scenario."

3 Communicate uncertainty in the timing of crossing impact-relevant thresholds

Extreme sea level AFs are often presented for an arbitrary future year in which the projection uncertainty in RSLC is only considered for that particular year (e.g., 2050, 2070, 2100). However, also of interest is analyzing projection uncertainty in the rates of RSLC and how it impacts the timing of reaching ESL frequency benchmarks, such as the first year in which the contemporary 100-yr ESL becomes the 1-yr ESL. Just as with assessing ESL AFs for particular years, impactful communication of the timing of such benchmarks should be tied to relevant societal thresholds, rather than arbitrary water levels. Examples include the year in which ESLs higher than the design height benchmark of protective infrastructure (e.g., the 100-yr water level) are expected to occur within the lifetime of that infrastructure (Rasmussen et al, 2020), or the population exposure associated with a given amount of RSLC. We use our simple ESL population exposure model to illustrate the latter.

The uncertainty in the timing of a doubling of the population exposed to the 100-yr ESL is illustrated for several global cities under a +2 °C scenario in Fig. 3 (all cities are given in the Supporting Data). Only uncertainty in the rates of RSLC are accounted for. For the Norfolk/Hampton Roads region, a doubling of the population exposure to the 100-yr ESL (∼16,000 people, corresponding to a RSLC of 0.32 m) is likely (17-83% probability) to occur between 2033 and 2051 under a +2 °C global mean temperature stabilization scenario (USA; Fig. 3C). For San Juan (Puerto Rico), a doubling of the population exposure to the 100-yr ESL is likely (17-83% probability) to occur much later, between 2088 and 2172 (Fig. 3C). Such temporal analyses as this can better inform long-term planning, including estimating lead-times for the completion of resilience measures needed to protect critical infrastructure (e.g., airports, power plants, and wastewater treatment facilities, Yesudian and Dawson, 2021; Bierkandt et al, 2015; Hummel et al, 2018).

While these analyses are local, they can be aggregated to regional or global scales to better inform aggregate statements about uncertainty in the timing of changes in ESLs. For example, using our analysis, a summary statement could be constructed that communicates uncertainty in the timing of population exposure

doubling, "projected 2070 RSLC under an end-of-century +2 °C GSAT stabilization scenario (relative to pre-industrial) is expected to at least double the 2010 population exposed to the 100-yr ESL before 2100 at 27% of the 414 coastal cities assessed. This fraction grows to 54% under an end-of-century +5 °C GSAT scenario." We note that considering population exposure produces drastically different summary statements from those given in SROCC that only consider the hazard, for example stating that "most" locations will experience the contemporary 100-yr ESL annually by 2100 (see Sec. 2). Furthermore, as opposed to "many" localities experiencing the contemporary 100-yr ESL annually by 2050 (as stated in SROCC), we find that under a +2 °C GSAT scenario, $< 7\%$ of the 414 cities from this study are expected to experience a doubling of the population exposure to the 100-yr ESL before 2050 ($\sim$12% under a +5 °C GSAT scenario). The focus on a doubling of population exposure is an arbitrary example; other societal thresholds could be explored.

4 Further suggestions for ways forward

Extreme Sea Level (ESL) frequency amplification factors (AFs) are easy-to-calculate metrics that can help communicate flood and sea-level rise risks when anchored to salient local events, such as the flooding of roadways, property, and other infrastructure (e.g., Sweet et al, 2018). However, stripped of their local context, ESL AFs only measure changes in arbitrary water levels at tide gauges that do not meaningfully aggregate to regional and global scales. In this essay, we have provided suggestions to improve ESL impact messaging in a regional or global-scale assessment. We make some further remarks here as well as give new research directions.

4.1 The IPCC and other assessment reports should leverage exposure and vulnerability datasets

To address the issue of contextualizing local ESL impacts at the global scale, we recommend the IPCC and other climate assessment reports integrate local exposure and vulnerability datasets that have global coverage into their quantitative analyses. Doing so will also facilitate constructing more definitive summary statements regarding ESL impacts. For example, the IPCC's SROCC "Summary for Policy Makers" gives a strong, but qualitative statement on projected ESL impacts, "[T]he increasing frequency of high water levels can have severe impacts in many locations depending on exposure" (IPCC, 2019). Future IPCC assessments should consider coastal flood risk assessment approaches that consider local hazard, exposure, and vulnerability on global scales (e.g., Hallegatte et al, 2013; Abadie et al, 2017; Hanson et al, 2011).

In this essay we have suggested alternative and additional summary statements that could be constructed from population exposure datasets to add more context to projected changes in ESL frequencies (Secs. 2 and 3). These are given as illustrative examples only. Employing sophisticated flood hazard modeling (e.g., Bates et al, 2021) and considering plausible socioeconomic shifts that affect exposure (e.g., population change from the Shared Socioeconomic Pathways or SSPs; O'Neill et al, 2014) could be used to construct similar statements. Because impacts can vary by return period, summary statements should also be made for both more frequent and rarer ESLs (e.g., the 10-yr and 500-yr ESLs, respectively).

While the inclusion of vulnerability and exposure data is possible for assessment reports that combine changes in hazards with impacts (e.g., IPCC SROCC, IPCC SR1.5, the U.S. NCA), it is likely to be challenging (if not impossible) to implement in the IPCC's main assessment reports (e.g., AR6). This is because physical projections are separated from societal impacts by design, the former appearing in the Working Group 1 report, ahead of societal impacts that are later released in Working Group 2. Because of this separation, changes in hazards are inherently provided without context until the Working Group 2 report is released. In the interim period between these two reports, scientists, the media, and the public are forced to make subjective judgements about the impacts of these hazard changes without their explicit quantification. This reflects a need for tighter integration among working groups in future assessment cycles.

4.2 Create and maintain new publicly available exposure and vulnerability datasets

New and existing datasets of terrain and flood protection elevation can help meet the needs of global assessment reports that seek to contextualize hazards. However, if there are gaps in the literature regarding these

data, assessment reports are unlikely to fill the need on their own. Some existing datasets could help. The continually updated Dynamic and Interactive Vulnerability Assessment database (DIVA) is a popular source of vulnerability and exposure data for global scale coastal flood risk assessments (Vafeidis et al, 2008; Hinkel et al, 2014; Brown et al, 2016; Kirezci et al, 2020; Jevrejeva et al, 2018; Muis et al, 2016; Wolff et al, 2016). This includes socio-economic data such as capital stock, tourism, and adaptation costs as well as ecological information such as coastal land type (e.g., wetlands, mangroves, beach) and erosion rates (Hinkel and Klein, 2009). However, most DIVA studies are economically oriented (e.g., appraising various adaptation approaches using benefit-cost analyses) and consider country or regional-level entities (the notable exception is Hallegatte et al, 2013). City-level information is arguably more relevant for informing decisions in countries that divide political power between local, state/provincial, and national levels (Den Uyl and Russel, 2018; Glicksman, 2010; Peterson, 1981). Furthermore, to our knowledge, DIVA is not publicly available. Therefore, it cannot be used for new integrative analyses done by the IPCC (see the FAIR data principles, Wilkinson et al, 2016; Juckes et al, 2020).

Large uncertainties in global exposure assessments are associated with the accuracy of digital elevation models (DEMs). New near-global scale DEMs have provided increased accuracy for population exposure assessments (e.g., CoastalDEM, MERIT, and NASADEM; Kulp and Strauss, 2019; Yamazaki et al, 2017). In the US, where high accuracy data derived from airborne lidar exists for which to validate these products, CoastalDEM's reported vertical error as measured by the root-mean squared error (RMSE) is 2.4 m, with considerable spatial variability. Given the importance of DEMs in flood risk assessment (McClean et al, 2020), further DEM accuracy improvements for these products are needed (Hinkel et al, 2021; Gesch, 2018). CoastalDEM[1], MERIT and NASADEM are publicly available.

Exposure is not always a good proxy for impacts, particularly in densely built environments where flood protection plays a significant role. Several populations living in low-lying areas around the world (e.g., deltaic regions) are protected by flood protection such as levees, seawalls, and deliberately raised structures (e.g., buildings on stilts; Scussolini et al, 2016; Nicholls et al, 2019). Just like previous flood exposure studies (Neumann et al, 2015; Hanson et al, 2011; Kulp and Strauss, 2019; McGranahan et al, 2007; Jongman et al, 2012; Lichter et al, 2011), our exposure estimates do not account for these protection tactics because they can be overtopped and breached. While this omission is common practice in exposure assessment (McClean et al, 2020), it is not always apparent to policy makers, stakeholders, and decision-makers who must interpret such information. In some cases, it has caused confusion from a communications standpoint (e.g., Mussen, 2021). While some efforts have been made[2], a spatially explicit global database with flood protection footprints, elevations/protection levels, and failure rates remains elusive (Hinkel et al, 2021).

Lastly, while population exposure is highlighted in this essay as a viable metric to communicate ESL impacts, all ESL metrics have limitations in terms of what impacts they communicate. For example, population exposure metrics that are a percent of the total city population ignore absolute numbers of people. Population vulnerability should be considered, including accounting for those who are least able to evacuate a flood event based on age, disability, poverty, and other cause of immobility (e.g., Hurricane Katrina, Eisenman et al, 2007). Other metrics with policy-relevance include projected increases in disaster aid and flood insurance claims, the credit worthiness of municipalities, and metrics that estimate when recovery from major floods begins to be cut short by new events (e.g., Otto et al, 2021). For example, despite Hurricane Sandy having occurred over eight years ago, the New York Metropolitan Transit Authority just completed repairing the damage suffered by New York City's subway system (Mass Transit Magazine, 2021). New research and publicly available datasets are needed in order to highlight these impacts. Advancements could be made through collaborations among researchers in climate adaptation, disaster risk management, and other relevant fields. Ultimately, the choice of which indicators and thresholds to highlight is subjective and depends on what stakeholders, the public, and policy makers view as being the most relevant for their needs.

Acknowledgements We thank William V. Sweet (NOAA) for stimulating conversations about the limitations of applying extreme sea level frequency amplification factors. D. J. R. was supported by both the Center for Policy Research on Energy and the

[1] the 90 meter resolution version only

[2] Hallegatte et al (2013) give upper and lower estimates of flood protection for over 100 major cities around the world based on surveyed responses from local experts. But this list is incomplete, these responses have not been verified, and local protection can also vary within a city. Tiggeloven et al (2020) use the FLOPROS modeling approach (Scussolini et al, 2016) to estimate flood protection, but these calculations have not been locally verified.

Environment (CPREE) and the Science, Technology, and Environmental Policy (STEP) Program at Princeton University. R. E. K. was supported by grants from the National Science Foundation (ICER-1663807, DGE-1633557), the National Aeronautics and Space Administration (80NSSC17K0698), and from the Rhodium Group (for whom he has previously worked as a consultant) as part of the Climate Impact Lab consortium. S. K. and B. H. S. were supported by National Science Foundation (ICER-1663807), the National Aeronautics and Space Administration (80NSSC17K0698), and the V. Kann Rasmussen Foundation. M. O. was supported by the National Science Foundation grant 1520683. The 3-arcsecond (90-m) version of CoastalDEM used in this analysis is available at no cost from Climate Central for non-commercial research use. Code for generating sea-level projections is available in the following repositories on Github: ProjectSL (https://github.com/bobkopp/ProjectSL) and LocalizeSL (https://github.com/bobkopp/LocalizeSL). Code for generating extreme sea level projections is available in the following repositories on Github: hawaiiSL_process (https://github.com/dmr2/hawaiiSL_process), GPDfit (https://github.com/dmr2/GPDfit), and return_curves (https://github.com/dmr2/return_curves). The statements, findings, conclusions, and recommendations are those of the authors and do not necessarily reflect the views of the funding agencies.

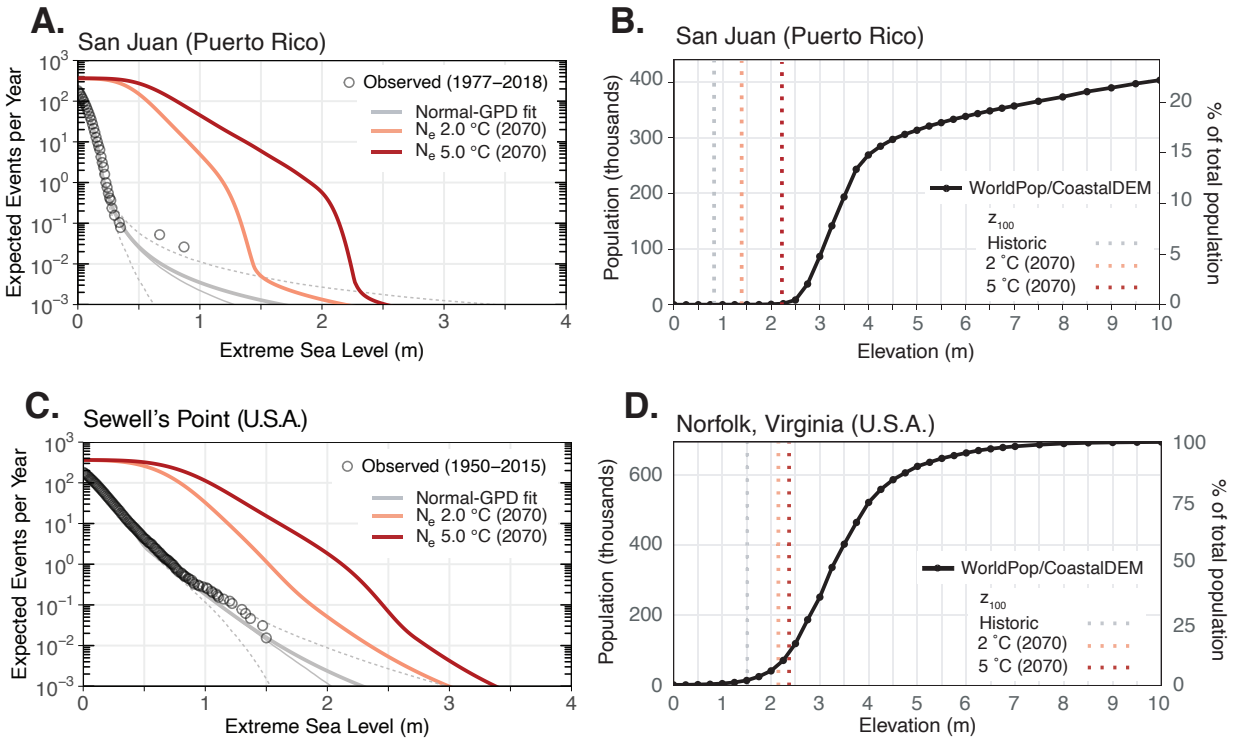

Fig. 1: **A.** Expected number of contemporary extreme sea level (ESL) events per year as a function of ESL height (meters above local mean higher high water; MHHW) calculated by fitting a Normal-generalized Pareto distribution (GPD) probability mixture model to tide gauge observations (open grey circles) at San Juan (Puerto Rico) for 1991–2009 local mean sea level (thick grey line), expected number of projected ESL events per year as a functions of projected relative sea-level change (RSLC) in 2070 under a scenario in which global mean surface air temperature (GSAT) is stabilized in 2100 at +2 °C (orange line) and +5 °C (red line; GSAT relative to 1850–1900). Thin grey lines are the contemporary ESL return curves for the 5/50/95 percentiles of the GPD parameter uncertainty range (dotted/solid/dotted lines, respectively). **B.** A population exposure function that estimates the total population (left y-axis) and percent of total population (right y-axis) currently exposed as a function of ESL height (meters above MHHW) for San Juan (total population: 1.82 million). Filled black circles are population data from the 2010 WorldPop global gridded population database (Tatem, 2017) applied to the elevation surfaces of CoastalDEM (Kulp and Strauss, 2018). Linear interpolation is used to produce a continuous curve between the WorldPop data (black line). City boundaries are those as defined by Kelso and Patterson (2012) and may differ from actual administrative borders. Populations are assumed to remain constant in time. Denoted is the height of the contemporary 100-yr ESL (grey), and the expected heights of the 100-yr ESL under a +2 °C (orange) and +5 °C (red) climate scenario. **C.** as for A., but for the Norfolk/Hampton Roads region of Virginia (U.S.A.). **D.** As for B., but for the Norfolk/Hampton Roads region of Virginia (U.S.A.; total population: 695,000).

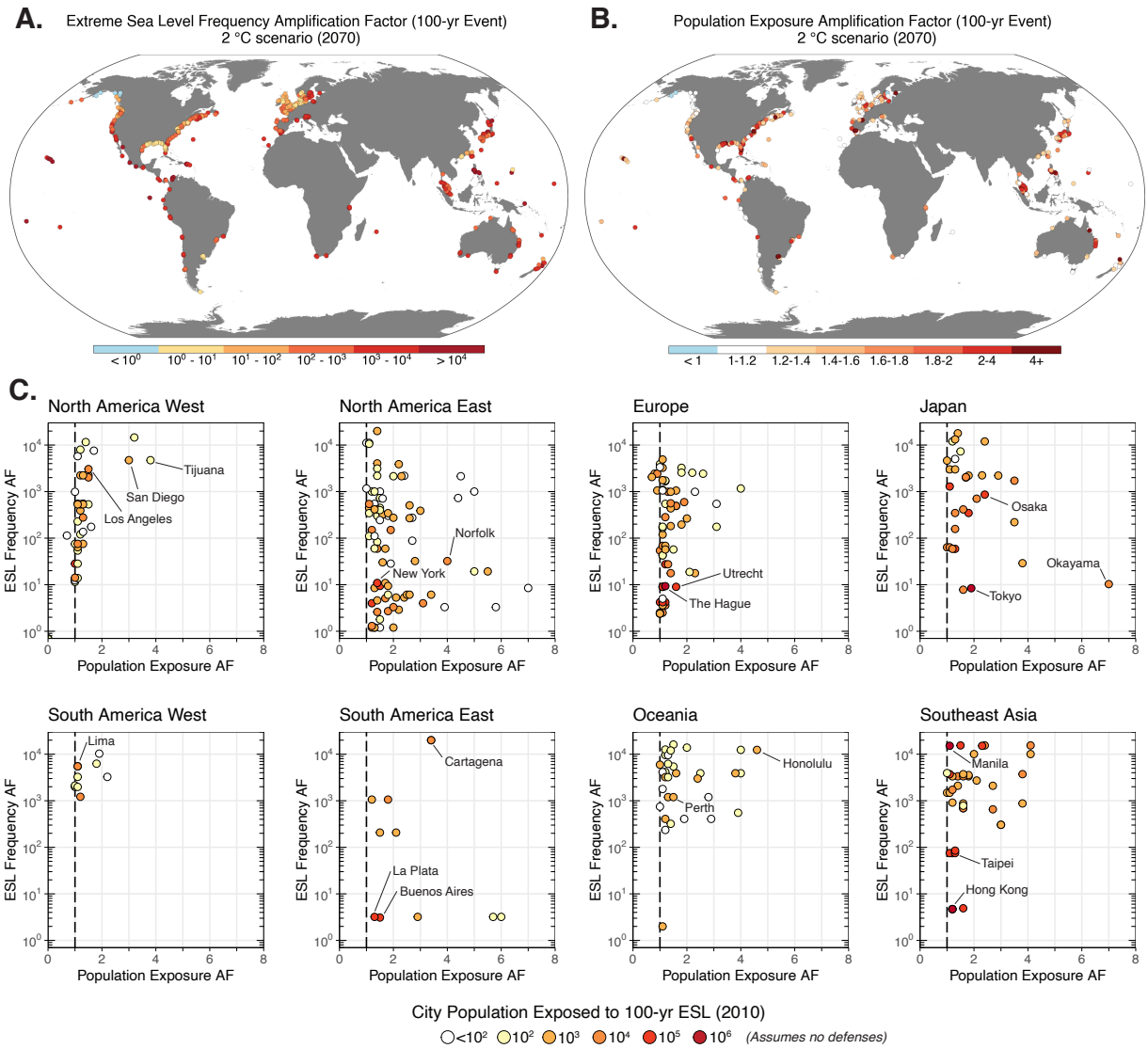

Fig. 2: **A.** Extreme sea level (ESL) frequency amplification factors (AFs) for cities for 2070 under a climate scenario where the global mean surface air temperature is stabilized in 2100 at +2 °C (relative to 1850–1900). **B.** As for A., but for population exposure AFs. Populations are assumed to remain constant in time. A population exposure AF of 1 indicates no change in exposure. **C.** ESL frequency AFs plotted against population exposure AFs for the 100-yr ESL for 2070 for the same climate scenario as the maps. The 2010 population exposed to the contemporary 100-yr ESL is indicated for each city. A list of the cities in each defined region is given in the supporting data files. Note that some cities may not appear in the scatter plots if 1) contemporary and projected population exposure to flood is zero, 2) the contemporary population exposure to flood is zero but projected exposure is non-zero (i.e., a population exposure AF of infinity), or 3) the population exposure AF is greater than two standard deviations from the mean of each region.

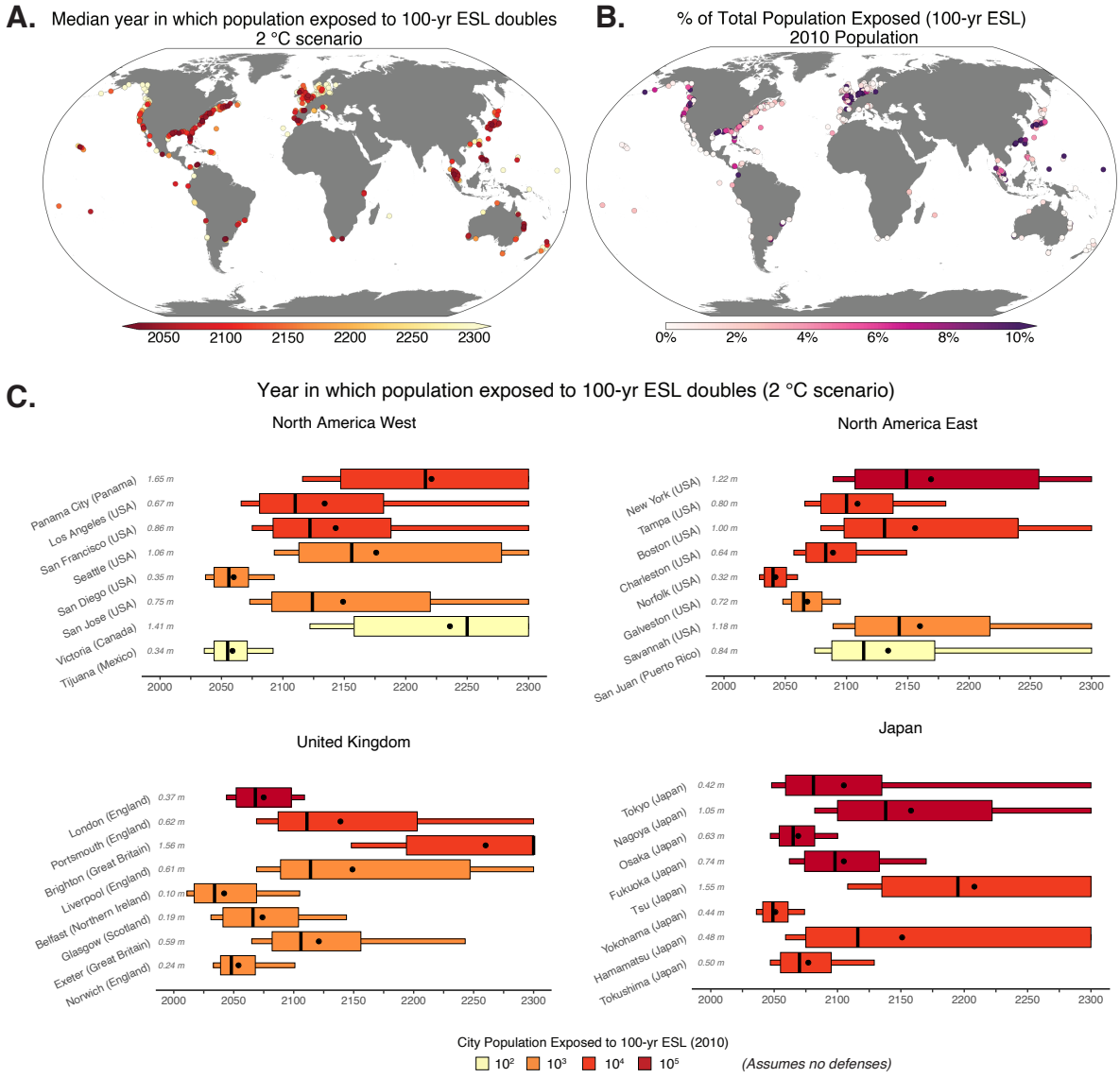

Fig. 3: **A.** Median projected year in which local relative sea-level change (RSLC) doubles the population exposure to the contemporary 100-yr extreme sea level (ESL) event (i.e., a population exposure amplification factor of 2; analysis assumes constant population) under a scenario in which global mean surface air temperature in 2100 is stabilized at +2 °C (relative to 1850–1900). **B.** Percent of the total city population exposed to the contemporary 100-yr ESL (assumes 2010 population). **C.** As for A, but highlighting select cities to show the RSLC uncertainty as a box plot. The thinner boxes cover the 5/95 percentile of RSLC uncertainty while the thicker boxes cover the 17/83 percentile. Black lines denote the 50th percentile and black dots denote the expected year. The RSLC amounts associated with each population exposure AF threshold are given in light grey (relative to 2000). The color of each box indicates the 2010 population exposure to the 100-yr ESL (assumes no flood defenses).

100-yr ESL event			2070 (2.0 °C)					
	Contemporary		Physical metrics		Societal metrics			
City (Total population in thousands)	100-yr ESL (m)	% Pop exposed	RSLC (m)	ESL frequency AF	Pop exposure AF	Pop exposed (thousands)	% Pop exposed	Pop doubling year
Buenos Aires, Argentina (11,980)	2.6 (2.1-3.3)	7.6%	0.4 (0.2-0.7)	3 (2-6)	1.5 (1.2-1.7)	1,328 (1,121-1,526)	11.1% (9.4-12.7%)	2211 (2110-2300)
Copenhagen, Denmark (1,337)	1.1 (1.0-1.1)	1.5%	0.2 (-0.8-1.1)	991 (0-9677)	1.3 (0.0-3.2)	26 (0-63)	1.9% (<0.1-4.7%)	2190 (2045-2300)
Dar es Salaam, Tanzania (2,322)	0.7 (0.6-0.7)	1.0%	0.5 (0.2-0.8)	2441 (254-6678)	1.7 (1.1-2.6)	39 (25-59)	1.7% (1.1-2.6%)	2086 (2052-2144)
Hamburg, Germany (1,854)	4.0 (3.6-4.3)	14.9%	0.4 (0.1-0.7)	4 (2-9)	1.1 (1.0-1.2)	301 (285-320)	16.2% (15.3-17.2%)	2300 (2300-2300)
Hong Kong, China (22,232)	1.8 (1.2-2.6)	33.1%	0.4 (0.1-0.8)	5 (1-12)	1.2 (1.1-1.4)	9,015 (7,788-10,131)	40.6% (35.0-45.6%)	2300 (2300-2300)
Honolulu, HI, USA (466)	0.4 (0.3-0.4)	0.5%	0.5 (0.2-0.9)	12385 (942-14455)	4.6 (2.1-8.5)	11 (5-20)	2.3% (1.0-4.2%)	2041 (2025-2065)
London, England (9,878)	0.9 (0.7-1.1)	1.8%	0.4 (0.2-0.7)	61 (4-188)	2.1 (1.4-2.9)	367 (252-515)	3.7% (2.5-5.2%)	2075 (2044-2109)
Manila, Philippines (5,782)	0.8 (0.7-0.9)	36.6%	0.9 (0.6-1.2)	15146 (3018–*)	1.1 (1.1-1.2)	2,339 (2,251-2,443)	40.5% (38.9-42.3%)	2300 (2300-2300)
New Orleans, LA, USA (711)	2.3 (1.2-4.2)	77.7%	1.0 (0.7-1.3)	4 (2-7)	1.2 (1.1-1.2)	643 (623-663)	90.4% (87.6-93.2%)	—
New York, NY, USA (12,520)	1.9 (1.5-2.3)	3.7%	0.6 (0.3-0.9)	11 (2-29)	1.4 (1.2-1.7)	653 (539-799)	5.2% (4.3-6.4%)	2169 (2089-2300)
Norfolk, VA, USA (695)	1.5 (1.1-1.9)	2.3%	0.6 (0.4-1.0)	32 (4-81)	4.0 (2.2-7.3)	64 (35-114)	9.2% (5.1-16.4%)	2042 (2029-2060)
Phuket, Thailand (159)	0.9 (0.8-1.0)	9.0%	0.5 (0.2-0.8)	1723 (37-7875)	1.2 (1.1-1.4)	17 (16-20)	11.0% (9.9-12.5%)	2204 (2104-2300)
Rio de Janeiro, Brazil (9,110)	0.9 (0.8-1.1)	0.3%	0.5 (0.2-0.8)	1061 (8-5808)	1.8 (1.3-2.5)	58 (41-79)	0.6% (0.5-0.9%)	2092 (2055-2165)
San Diego, CA, USA (2,323)	0.7 (0.7-0.7)	0.2%	0.5 (0.2-0.8)	4726 (298-15431)	3.0 (1.6-5.7)	13 (7-25)	0.6% (0.3-1.1%)	2060 (2037-2093)
San Juan, Puerto Rico (1,821)	0.7 (0.5-1.1)	0.0%	0.5 (0.2-0.8)	3130 (4–*)	1.4 (1.1-1.9)	<1 (<1- <1)	<0.1% (<0.1- <0.1%)	2134 (2074-2300)
Shenzhen, China (12,518)	1.8 (1.2-2.6)	17.5%	0.4 (0.1-0.8)	5 (1-12)	1.2 (1.1-1.3)	2,649 (2,314-2,938)	21.2% (18.5-23.5%)	2300 (2300-2300)
Sydney, Australia (3,483)	0.7 (0.7-0.7)	0.2%	0.4 (0.2-0.8)	3213 (60-16480)	1.2 (1.1-1.3)	9 (9-11)	0.3% (0.2-0.3%)	2177 (2090-2300)
Tokyo, Japan (25,339)	1.5 (1.0-2.1)	5.5%	0.4 (0.1-0.7)	8 (1-18)	1.9 (1.1-3.0)	2,651 (1,610-4,278)	10.5% (6.4-16.9%)	2105 (2048-2300)
Vancouver, Canada (1,810)	1.3 (1.1-1.6)	11.8%	0.2 (0.0-0.5)	28 (1-94)	1.0 (1.0-1.0)	218 (214-223)	12.0% (11.8-12.3%)	2300 (2300-2300)

Table 1: Table listing both physical and societal extreme sea level (ESL) metrics for select major coastal cities. Given are the heights of the contemporary 100-yr ESL return period (meters relative to mean higher high water; expected/5th/95th percentile), the percent of the total population exposed to the expected 100-yr ESL, 2070 probabilistic relative sea-level change (RSLC) (meters, relative to 1991–2009) from a climate scenario in which global mean surface air temperature (GSAT) is stabilized in 2100 at +2 °C (relative to 1850–1900; Bamber et al, 2019), ESL return period amplification factors (AFs) for the 100-yr ESL, the population exposure AF, the estimated total population exposed to the projected 100-yr ESL (thousands), the same number as a percent of the total population, and the year in which the population exposed to the 100-yr ESL doubles. The expected value and the 5/95 percentile of the estimate are given for each. The 5/95 percentile for the contemporary ESL return period considers the uncertainty in the generalized Pareto distribution (GPD) parameters, while the 5/95 percentile for RSLC and AFs reflect the uncertainty from both contributions to local RSLC and from the GPD. The * denotes instances of when the height of the contemporary 100-yr ESL occurs more often than the present-day frequency of exceeding MHHW (given for each tide gauge in the supporting information). The mapping of tide gauges to cities is given in the supporting information.

References

Abadie LM, Galarraga I, De Murieta ES (2017) Understanding risks in the light of uncertainty: Low-probability, high-impact coastal events in cities. Environmental Research Letters 12(1), DOI 10.1088/1748-9326/aa5254

Arns A, Dangendorf S, Jensen J, et al (2017) Sea-level rise induced amplification of coastal protection design heights. Scientific Reports 7(1):40,171, DOI 10.1038/srep40171

Arns A, Wahl T, Wolff C, et al (2020) Non-linear interaction modulates global extreme sea levels, coastal flood exposure, and impacts. Nature Communications 11(1):1918, DOI 10.1038/s41467-020-15752-5

Bamber JL, Oppenheimer M, Kopp RE, Aspinall WP, Cooke RM (2019) Ice sheet contributions to future sea-level rise from structured expert judgment. Proceedings of the National Academy of Sciences 116(23):11,195–11,200, DOI 10.1073/pnas.1817205116

Baranes HE, Woodruff JD, Talke SA, et al (2020) Tidally Driven Interannual Variation in Extreme Sea Level Frequencies in the Gulf of Maine. Journal of Geophysical Research: Oceans 125(10):e2020JC016,291, DOI https://doi.org/10.1029/2020JC016291, URL http://agupubs.onlinelibrary.wiley.com/doi/abs/10.1029/2020JC016291, _eprint: https://onlinelibrary.wiley.com/doi/pdf/10.1029/2020JC016291

Bates PD, Dawson RJ, Hall JW, et al (2005) Simplified two-dimensional numerical modelling of coastal flooding and example applications. Coastal Engineering 52(9):793–810, DOI 10.1016/j.coastaleng.2005.06.001, URL https://linkinghub.elsevier.com/retrieve/pii/S037838390500075X

Bates PD, Quinn N, Sampson C, et al (2021) Combined Modeling of US Fluvial, Pluvial, and Coastal Flood Hazard Under Current and Future Climates. Water Resources Research 57(2):e2020WR028,673, DOI https://doi.org/10.1029/2020WR028673

Behrens CN, Lopes HF, Gamerman D (2004) Bayesian analysis of extreme events with threshold estimation. Statistical Modelling 4(3):227–244, DOI 10.1191/1471082X04st075oa, URL http://journals.sagepub.com/doi/10.1191/1471082X04st075oa

Bierkandt R, Auffhammer M, Levermann A (2015) US power plant sites at risk of future sea-level rise. Environmental Research Letters 10(12):124,022, DOI 10.1088/1748-9326/10/12/124022, URL https://iopscience.iop.org/article/10.1088/1748-9326/10/12/124022

Breilh JF, Chaumillon E, Bertin X, Gravelle M (2013) Assessment of static flood modeling techniques: application to contrasting marshes flooded during Xynthia (western France). Natural Hazards and Earth System Sciences 13(6):1595–1612, DOI 10.5194/nhess-13-1595-2013, URL https://nhess.copernicus.org/articles/13/1595/2013/

Brown S, Nicholls RJ, Lowe JA, Hinkel J (2016) Spatial variations of sea-level rise and impacts: An application of DIVA. Climatic Change 134(3):403–416, DOI 10.1007/s10584-013-0925-y, URL https://doi.org/10.1007/s10584-013-0925-y

Buchanan MK, Kopp RE, Oppenheimer M, Tebaldi C (2016) Allowances for evolving coastal flood risk under uncertain local sea-level rise. Climatic Change DOI 10.1007/s10584-016-1664-7

Buchanan MK, Oppenheimer M, Kopp RE (2017) Amplification of flood frequencies with local sea level rise and emerging flood regimes. Environmental Research Letters 12(6), DOI 10.1088/1748-9326/aa6cb3

Caldwell PC, Merrifield MA, Thompson PR (2015) Sea level measured by tide gauges from global oceans — the Joint Archive for Sea Level holdings (NCEI Accession 0019568). NOAA National Centers for Environmental Information Dataset

Church JA, Clark PU, et al (2013) Chapter 13: Sea level change. In: Stocker TF, Qin D, Plattner GK, et al (eds) Climate Change 2013: the Physical Science Basis, Cambridge University Press

Coles S (2001a) Classical Extreme Value Theory and Models. In: An Introduction to Statistical Modeling of Extreme Values, Springer, chap 3

Coles S (2001b) An Introduction to Statistical Modeling of Extreme Values. Springer-Verlag London, London, UK, URL https://books.google.com/books?id=2nugUEaKqFEC, series Title: Lecture Notes in Control and Information Sciences

Coles S (2001c) Threshold Models. In: An Introduction to Statistical Modeling of Extreme Values, Springer, chap 4

Coles SG, Powell EA (1996) Bayesian Methods in Extreme Value Modelling: A Review and New Developments. International Statistical Review / Revue Internationale de Statistique 64(1):119–136, DOI 10.2307/1403426, URL http://www.jstor.org/stable/1403426, publisher: [Wiley, International Statis-

tical Institute (ISI)]

Coles SG, Tawn JA (1994) Statistical Methods for Multivariate Extremes: An Application to Structural Design. Journal of the Royal Statistical Society Series C (Applied Statistics) 43(1):1–48, DOI 10.2307/2986112, URL http://www.jstor.org/stable/2986112, publisher: [Wiley, Royal Statistical Society]

Coles SG, Tawn JA (1996) Modelling Extremes of the Areal Rainfall Process. Journal of the Royal Statistical Society Series B (Methodological) 58(2):329–347, URL http://www.jstor.org/stable/2345980, publisher: [Royal Statistical Society, Wiley]

Cunnane C (1973) A particular comparison of annual maxima and partial duration series methods of flood frequency prediction. Journal of Hydrology 18(3-4):257–271, DOI 10.1016/0022-1694(73)90051-6

Dahl KA, Fitzpatrick MF, Spanger-Siegfried E (2017) Sea level rise drives increased tidal flooding frequency at tide gauges along the U.S. East and Gulf Coasts: Projections for 2030 and 2045. PLOS ONE 12(2):e0170,949, DOI 10.1371/journal.pone.0170949, URL https://journals.plos.org/plosone/article?id=10.1371/journal.pone.0170949, publisher: Public Library of Science

Davison AC, Smith RL (1990) Models for Exceedances over High Thresholds. Journal of the Royal Statistical Society Series B (Methodological) 52(3):393–442, URL http://www.jstor.org/stable/2345667, publisher: [Royal Statistical Society, Wiley]

Den Uyl RM, Russel DJ (2018) Climate adaptation in fragmented governance settings: the consequences of reform in public administration. Environmental Politics 27(2):341–361, DOI 10.1080/09644016.2017.1386341

DuMouchel WH (1983) Estimating the Stable Index α in Order to Measure Tail Thickness: A Critique. The Annals of Statistics 11(4):1019–1031, DOI 10.1214/aos/1176346318, URL https://projecteuclid.org/journals/annals-of-statistics/volume-11/issue-4/Estimating-the-Stable-Index-alpha-in-Order-to-Measure-Tail/10.1214/aos/1176346318.full, publisher: Institute of Mathematical Statistics

Dupuis D (1998) Exceedances over High Thresholds: A Guide to Threshold Selection. Extremes 1(3):251–261

Egbert GD, Erofeeva SY (2002) Efficient inverse modeling of barotropic ocean tides. Journal of Atmospheric and Oceanic Technology 19(2):183–204, DOI 10.1175/1520-0426(2002)019

Eisenman DP, Cordasco KM, Asch S, Golden JF, Glik D (2007) Disaster planning and risk communication with vulnerable communities: Lessons from hurricane katrina. American Journal of Public Health 97(S1):S109–S115, DOI 10.2105/AJPH.2005.084335

Embrechts P, Klüppelberg C, Mikosch T (1997) Modelling Extremal Events. Springer Berlin Heidelberg, Berlin, Heidelberg, DOI 10.1007/978-3-642-33483-2, URL http://link.springer.com/10.1007/978-3-642-33483-2

Familkhalili R, Talke SA (2016) The effect of channel deepening on tides and storm surge: A case study of Wilmington, NC. Geophysical Research Letters 43(17):9138–9147, DOI 10.1002/2016GL069494, URL https://agupubs.onlinelibrary.wiley.com/doi/abs/10.1002/2016GL069494, _eprint: https://agupubs.onlinelibrary.wiley.com/doi/pdf/10.1002/2016GL069494

Farr TG, Rosen PA, Caro E, et al (2007) The Shuttle Radar Topography Mission. Reviews of Geophysics 45(2), DOI 10.1029/2005RG000183

Feng J, Li H, Li D, et al (2018) Changes of Extreme Sea Level in 1.5 and 2.0°c Warmer Climate Along the Coast of China. Frontiers in Earth Science 6:216, DOI 10.3389/feart.2018.00216, URL https://www.frontiersin.org/article/10.3389/feart.2018.00216/full

Fox-Kemper B, Hewitt HT, Xiao C, et al (2021) Chapter 9: Ocean, Cryosphere and Sea Level Change. In: Masson-Delmotte V, Zhai P, Pirani A, et al (eds) Climate Change 2021: The Physical Science Basis. Contribution of Working Group I to the Sixth Assessment Report of the Intergovernmental Panel on Climate Change, Intergovernmental Panel on Climate Change (IPCC)

Frederikse T, Buchanan MK, Lambert E, et al (2020) Antarctic Ice Sheet and emission scenario controls on 21st-century extreme sea-level changes. Nature Communications 11(1):1–11, DOI 10.1038/s41467-019-14049-6

Gallien T (2016) Validated coastal flood modeling at Imperial Beach, California: Comparing total water level, empirical and numerical overtopping methodologies. Coastal Engineering 111:95–104, DOI 10.1016/j.coastaleng.2016.01.014, URL https://linkinghub.elsevier.com/retrieve/pii/S0378383916300059

Garner AJ, Mann ME, Emanuel KA, et al (2017) Impact of climate change on New York City's coastal flood hazard: Increasing flood heights from the preindustrial to 2300 CE. PNAS pp 1–6, DOI 10.1073/pnas.

1703568114
Gesch DB (2018) Best Practices for Elevation-Based Assessments of Sea-Level Rise and Coastal Flooding Exposure. Frontiers in Earth Science 6, DOI 10.3389/feart.2018.00230, publisher: Frontiers
Ghanbari M, Arabi M, Obeysekera J, Sweet W (2019) A Coherent Statistical Model for Coastal Flood Frequency Analysis Under Nonstationary Sea Level Conditions. Earth's Future DOI 10.1029/2018EF001089
Glicksman RL (2010) Climate change adaptation: A collective action perspective on federalism considerations. Environmental Law 40(4):1159–1193
Gregory JM, Griffies SM, Hughes CW, et al (2019) Concepts and Terminology for Sea Level: Mean, Variability and Change, Both Local and Global. Surveys in Geophysics 40(6):1251–1289, DOI 10.1007/s10712-019-09525-z
Hallegatte S, Green C, Nicholls RJ, Corfee-Morlot J (2013) Future flood losses in major coastal cities. Nature Climate Change 3(9):802–806, DOI 10.1038/nclimate1979
Hanson S, Nicholls R, Ranger N, et al (2011) A global ranking of port cities with high exposure to climate extremes. Climatic Change 104(1):89–111, DOI 10.1007/s10584-010-9977-4
Hauer ME (2017) Migration induced by sea-level rise could reshape the us population landscape. Nature Clim Change 7(5):321–325, URL http://dx.doi.org/10.1038/nclimate3271
Hauer ME, Evans JM, Mishra DR (2016) Millions projected to be at risk from sea-level rise in the continental United States. Nat Clim Chang (March), DOI 10.1038/nclimate2961, URL http://www.nature.com/doifinder/10.1038/nclimate2961
Hausfather Z, Peters GP (2020) Emissions – the 'business as usual' story is misleading. Nature 577(7792):618–620, DOI 10.1038/d41586-020-00177-3
Hinkel J, Klein RJ (2009) Integrating knowledge to assess coastal vulnerability to sea-level rise: The development of the DIVA tool. Global Environmental Change 19(3):384–395, DOI 10.1016/j.gloenvcha.2009.03.002, URL https://linkinghub.elsevier.com/retrieve/pii/S0959378009000247
Hinkel J, Lincke D, Vafeidis AT, et al (2014) Coastal flood damage and adaptation costs under 21st century sea-level rise. Proceedings of the National Academy of Sciences of the United States of America 111(9):3292–7, DOI 10.1073/pnas.1222469111
Hinkel J, Feyen L, Hemer M, et al (2021) Uncertainty and Bias in Global to Regional Scale Assessments of Current and Future Coastal Flood Risk. Earth's Future 9(7), DOI 10.1029/2020EF001882, URL https://onlinelibrary.wiley.com/doi/10.1029/2020EF001882
Hoegh-Guldberg O, Jacob D, Taylor M, et al (2018) Impacts of 1.5°C of Global Warming on Natural and Human Systems. In: Masson-Delmotte V, Zhai P, Pörtner HO, et al (eds) Global Warming of 1.5°C. An IPCC Special Report on the impacts of global warming of 1.5°C above pre-industrial levels and related global greenhouse gas emission pathways, in the context of strengthening the global response to the threat of climate change, sustainable development, and efforts to eradicate poverty, Cambridge, p 138
Howard T, Palmer MD (2020) Sea-level rise allowances for the UK. Environmental Research Communications 2(3):035,003, DOI 10.1088/2515-7620/ab7cb4, URL https://doi.org/10.1088%2F2515-7620%2Fab7cb4, publisher: IOP Publishing
Hummel MA, Berry MS, Stacey MT (2018) Sea Level Rise Impacts on Wastewater Treatment Systems Along the U.S. Coasts. Earth's Future 6(4):622–633, DOI 10.1002/2017EF000805, URL https://agupubs.onlinelibrary.wiley.com/doi/abs/10.1002/2017EF000805, _eprint: https://agupubs.onlinelibrary.wiley.com/doi/pdf/10.1002/2017EF000805
Hunter J (2012) A simple technique for estimating an allowance for uncertain sea-level rise. Climatic Change 113:239–252, DOI 10.1007/s10584-011-0332-1
Hunter JR, Woodworth PL, Wahl T, Nicholls RJ (2017) Using global tide gauge data to validate and improve the representation of extreme sea levels in flood impact studies. Global and Planetary Change 156:34–45, DOI 10.1016/j.gloplacha.2017.06.007
IPCC (2019) Summary for Policy Makers. In: Pörtner HO, Roberts D, Masson-Delmotte V, et al (eds) IPCC Special Report on the Ocean and Cryosphere in a Changing Climate, Intergovernmental Panel on Climate Change (IPCC)
Jevrejeva S, Jackson LP, Grinsted A, Lincke D, Marzeion B (2018) Flood damage costs under the sea level rise with warming of 1.5 °C and 2.0 °C. Environ Res Lett 13(074014):11, DOI 10.1088/1748-9326/aacc76
Jongman B, Ward PJ, Aerts JCJH (2012) Global exposure to river and coastal flooding: Long term trends and changes. Global Environmental Change 22(4):823–835, DOI 10.1016/j.gloenvcha.2012.07.004, URL

http://www.sciencedirect.com/science/article/pii/S0959378012000830
Juckes M, Pirani A, Pascoe C, et al (2020) Implementing FAIR Principles in the IPCC Assessment Process. In: EGU General Assembly Conference Abstracts, EGU General Assembly
Kelso NV, Patterson T (2012) World Urban Areas, LandScan, 1:10 million
Kirezci E, Young IR, Ranasinghe R, et al (2020) Projections of global-scale extreme sea levels and resulting episodic coastal flooding over the 21st Century. Scientific Reports 10(1):11,629, DOI 10.1038/s41598-020-67736-6, URL https://www.nature.com/articles/s41598-020-67736-6, number: 1 Publisher: Nature Publishing Group
Kopp RE, Horton RM, Little CM, et al (2014) Probabilistic 21st and 22nd century sea-level projections at a global network of tide gauge sites. Earth's Future 2:383–406, DOI 10.1002/2014EF000239
Kopp RE, Gilmore EA, Little CM, et al (2019) Usable Science for Managing the Risks of Sea-Level Rise. Earth's Future 7(12):1235–1269, DOI 10.1029/2018EF001145
Kulp S, Strauss BH (2017) Rapid escalation of coastal flood exposure in US municipalities from sea level rise. Climatic Change 142(3-4):477–489, DOI 10.1007/s10584-017-1963-7
Kulp SA, Strauss BH (2018) CoastalDEM: A global coastal digital elevation model improved from SRTM using a neural network. Remote Sensing of Environment 206:231–239, DOI 10.1016/j.rse.2017.12.026
Kulp SA, Strauss BH (2019) New elevation data triple estimates of global vulnerability to sea-level rise and coastal flooding. Nature Communications 10(1):4844, DOI 10.1038/s41467-019-12808-z
Lang M, Ouarda TBMJ, Bobée B (1999) Towards operational guidelines for over-threshold modeling. Journal of Hydrology 225(3):103–117, DOI 10.1016/S0022-1694(99)00167-5
Lichter M, Vafeidis AT, Nicholls RJ (2011) Exploring Data-Related Uncertainties in Analyses of Land Area and Population in the "Low-Elevation Coastal Zone" (LECZ). Journal of Coastal Research 27(4):757–768, DOI 10.2112/JCOASTRES-D-10-00072.1, URL https://bioone.org/journals/journal-of-coastal-research/volume-27/issue-4/JCOASTRES-D-10-00072.1/Exploring-Data-Related-Uncertainties-in-Analyses-of-Land-Area-and/10.2112/JCOASTRES-D-10-00072.1.full
Little CM, Horton RM, Kopp RE, et al (2015) Joint projections of US East Coast sea level and storm surge. Nature Climate Change 5(12):1114–1120, DOI 10.1038/nclimate2801, URL http://www.scopus.com/inward/record.url?eid=2-s2.0-84948163996&partnerID=tZOtx3y1
MacDonald A, Scarrott C, Lee D, et al (2011) A flexible extreme value mixture model. Computational Statistics & Data Analysis 55(6):2137–2157, DOI 10.1016/j.csda.2011.01.005, URL https://linkinghub.elsevier.com/retrieve/pii/S0167947311000077
Mass Transit Magazine (2021) MTA announces completion of Sandy Resiliency work in F Line's East River tunnel. URL https://www.masstransitmag.com/rail/infrastructure/press-release/21216884/mta-new-york-city-transit-mta-announces-completion-of-sandy-resiliency-work-in-f-lines-east-river-tu
McClean F, Dawson R, Kilsby C (2020) Implications of Using Global Digital Elevation Models for Flood Risk Analysis in Cities. Water Resources Research 56(10):e2020WR028,241, DOI 10.1029/2020WR028241
McGranahan G, Balk D, Anderson B (2007) The rising tide: assessing the risks of climate change and human settlements in low elevation coastal zones. Environment and Urbanization 19(1):17–37, DOI 10.1177/0956247807076960, URL https://doi.org/10.1177/0956247807076960, publisher: SAGE Publications Ltd
Melet A, Meyssignac B, Almar R, Le Cozannet G (2018) Under-estimated wave contribution to coastal sea-level rise. Nature Climate Change 8(3):234–239, DOI 10.1038/s41558-018-0088-y
Menéndez M, Woodworth PL (2010) Changes in extreme high water levels based on a quasi-global tide-gauge data set. Journal of Geophysical Research: Oceans 115(10):1–15, DOI 10.1029/2009JC005997, iSBN: 2156-2202
Merkens JL, Reimann L, Hinkel J, Vafeidis AT (2016) Gridded population projections for the coastal zone under the Shared Socioeconomic Pathways. Global and Planetary Change 145:57–66, DOI 10.1016/j.gloplacha.2016.08.009, URL http://dx.doi.org/10.1016/j.gloplacha.2016.08.009
Moftakhari HR, Salvadori G, AghaKouchak A, Sanders BF, Matthew RA (2017) Compounding effects of sea level rise and fluvial flooding. Proceedings of the National Academy of Sciences DOI 10.1073/pnas.1620325114, URL http://www.pnas.org/content/early/2017/08/22/1620325114.abstract
Muis S, Verlaan M, Winsemius HC, Aerts JC, Ward PJ (2016) A global reanalysis of storm surge and extreme sea levels (1979-2014). Nature Communications 7(May):1–11, DOI 10.1038/ncomms11969

Muis S, Verlaan M, Nicholls RJ, et al (2017) A comparison of two global datasets of extreme sea levels and resulting flood exposure. Earth's Future 5(4):379–392, DOI 10.1002/2016EF000430

Mussen M (2021) These iconic London tourist attractions could be underwater in 30 years, including the Houses of Parliament and Tate Britain. URL https://www.mylondon.news/news/zone-1-news/iconic-london-tourist-attractions-could-20251869

Neumann B, Vafeidis AT, Zimmermann J, Nicholls RJ (2015) Future coastal population growth and exposure to sea-level rise and coastal flooding - A global assessment. PLoS One 10(3), DOI 10.1371/journal.pone.0118571

Nicholls RJ, Hanson S, Herweijer C, et al (2008) Ranking Port Cities with High Exposure and Vulnerability to Climate Extremes: Exposure Estimates. OECD Environment Working Papers No. 1, Organisation for Economic Co-operation and Development (OECD), Paris, France

Nicholls RJ, Hinkel J, Lincke D, van der Pol T (2019) Global Investment Costs for Coastal Defense through the 21st Century. World Bank Policy Research Working Paper 8745, World Bank Group, URL http://documents.worldbank.org/curated/en/433981550240622188/Global-Investment-Costs-for-Coastal-Defense-through-the-21st-Century

NOAA (2020) NOAA Digital Coast Coastal Lidar. URL https://coast.noaa.gov/digitalcoast/

O'Neill BC, Kriegler E, Riahi K, et al (2014) A new scenario framework for climate change research: the concept of shared socioeconomic pathways. Climatic Change 122:387–400, DOI 10.1007/s10584-013-0905-2

Oppenheimer M, Glavovic B, Hinkel J, et al (2019) Chapter 4: Sea level rise and implications for low lying islands, coasts and communities. In: Pörtner HO, Roberts D, Masson-Delmotte V, et al (eds) IPCC Special Report on the Ocean and Cryosphere in a Changing Climate, Intergovernmental Panel on Climate Change (IPCC)

Otto C, Kuhla K, Geiger T, Schewe J, Frieler K (2021) Incomplete recovery to enhance economic growth losses from U.S. hurricanes under global warming. Preprint DOI 10.21203/rs.3.rs-654258/v1

Parker B, Hess K, Milbert D, Gill S (2003) A national vertical datum transformation tool. Sea Technology 44(9):10–15

Peterson PE (1981) City Limits, 1st edn. University of Chicago Press, Chicago & London

Pickens J (1975) Statistical Inference Using Extreme Order Statistics. The Annals of Statistics 3(1):119–131, DOI 10.1214/aos/1176343003

Pugh D, Woodworth P (2014) Sea-Level Science: Understanding Tides, Surges, Tsunamis and Mean Sea-Level Changes, 2nd edn. Cambridge University Press, Cambridge, UK

Ramirez JA, Lichter M, Coulthard TJ, Skinner C (2016) Hyper-resolution mapping of regional storm surge and tide flooding: comparison of static and dynamic models. Natural Hazards 82(1):571–590, DOI 10.1007/s11069-016-2198-z, URL http://link.springer.com/10.1007/s11069-016-2198-z

Rasmussen DJ, Bittermann K, Buchanan MK, et al (2018) Extreme sea level implications of 1.5 °C, 2.0 °C, and 2.5 °C temperature stabilization targets in the 21st and 22nd centuries. Environmental Research Letters 13(3):034,040, DOI 10.1088/1748-9326/aaac87

Rasmussen DJ, Buchanan MK, Kopp RE, Oppenheimer M (2020) A Flood Damage Allowance Framework for Coastal Protection With Deep Uncertainty in Sea Level Rise. Earth's Future 8(3), DOI 10.1029/2019EF001340

Rasmussen DJ, Kopp RE, Shwom R, Oppenheimer M (2021) The Political Complexity of Coastal Flood Risk Reduction: Lessons for Climate Adaptation Public Works in the U.S. Earth's Future 9(2):e2020EF001,575, DOI 10.1029/2020EF001575

Rowan KE (1991) Goals, obstacles, and strategies in risk communication: A problem-solving approach to improving communication about risks. Journal of Applied Communication Research 19(4):300–329, DOI 10.1080/00909889109365311, URL http://www.tandfonline.com/doi/abs/10.1080/00909889109365311

Schindelegger M, Green JaM, Wilmes SB, Haigh ID (2018) Can We Model the Effect of Observed Sea Level Rise on Tides? Journal of Geophysical Research: Oceans 123(7):4593–4609, DOI 10.1029/2018JC013959, URL https://agupubs.onlinelibrary.wiley.com/doi/abs/10.1029/2018JC013959, _eprint: https://agupubs.onlinelibrary.wiley.com/doi/pdf/10.1029/2018JC013959

Scussolini P, Aerts JCJH, Jongman B, et al (2016) FLOPROS: an evolving global database of flood protection standards. Natural Hazards and Earth System Sciences 16(5):1049–1061, DOI 10.5194/nhess-16-1049-2016, URL https://nhess.copernicus.org/articles/16/1049/2016/

Seenath A, Wilson M, Miller K (2016) Hydrodynamic versus GIS modelling for coastal flood vulnerability assessment: Which is better for guiding coastal management? Ocean & Coastal Management 120:99–109, DOI 10.1016/j.ocecoaman.2015.11.019, URL https://linkinghub.elsevier.com/retrieve/pii/S0964569115300685

Sobel AH, Camargo SJ, Hall TM, et al (2016) Human influence on tropical cyclone intensity. Science 353(6296):242–246, DOI 10.1126/science.aaf6574, URL http://science.sciencemag.org/content/353/6296/242, http://science.sciencemag.org/content/353/6296/242.full.pdf

Sweet WV, Park J (2014) From the extreme to the mean: Acceleration and tipping points of coastal inundation from sea level rise. Earth's Future 2(12):579–600, DOI 10.1002/2014EF000272, 2014EF000272

Sweet WV, Kopp RE, Weaver CP, et al (2017) Global and regional sea level rise scenarios for the United States. Technical Report NOS CO-OPS 083, National Oceanic and Atmospheric Administration

Sweet WV, Dusek G, Obeysekera J, Marra JJ (2018) Patterns and Projections of High Tide Flooding Along the U.S. Coastline Using a Common Impact Threshold. NOAA Tech. Rep. NOS CO-OPS 086, National Oceanic and Atmospheric Administration, Silver Spring, MD

Taherkhani M, Vitousek S, Barnard PL, et al (2020) Sea-level rise exponentially increases coastal flood frequency. Scientific Reports 10(1):1–17, DOI 10.1038/s41598-020-62188-4

Talke SA, Orton P, Jay DA (2014) Increasing storm tides in New York Harbor, 1844–2013. Geophysical Research Letters 41(9):3149–3155, DOI 10.1002/2014GL059574, URL https://agupubs.onlinelibrary.wiley.com/doi/abs/10.1002/2014GL059574, _eprint: https://agupubs.onlinelibrary.wiley.com/doi/pdf/10.1002/2014GL059574

Tatem AJ (2017) WorldPop, open data for spatial demography. Scientific Data 4(1):1–4, DOI 10.1038/sdata.2017.4

Tebaldi C, Strauss BH, Zervas CE (2012) Modelling sea level rise impacts on storm surges along US coasts. Environmental Research Letters 7:014,032, DOI 10.1088/1748-9326/7/1/014032

Tiggeloven T, de Moel H, Winsemius HC, et al (2020) Global-scale benefit–cost analysis of coastal flood adaptation to different flood risk drivers using structural measures. Natural Hazards and Earth System Sciences 20(4):1025–1044, DOI 10.5194/nhess-20-1025-2020, URL https://nhess.copernicus.org/articles/20/1025/2020/, publisher: Copernicus GmbH

UNFCCC (2015) Report of the Conference of the Parties on its twenty-first session, held in Paris from 30 November to 13 December 2015, UNFCCC

Vafeidis AT, Nicholls RJ, McFadden L, et al (2008) A New Global Coastal Database for Impact and Vulnerability Analysis to Sea-Level Rise. Journal of Coastal Research 244:917–924, DOI 10.2112/06-0725.1, URL http://www.bioone.org/doi/abs/10.2112/06-0725.1

Vitousek S, Barnard PL, Fletcher CH, et al (2017) Doubling of coastal flooding frequency within decades due to sea-level rise. Scientific Reports 7(1):1–9, DOI 10.1038/s41598-017-01362-7

Vousdoukas MI, Voukouvalas E, Mentaschi L, et al (2016) Developments in large-scale coastal flood hazard mapping. Natural Hazards and Earth System Sciences 16(8):1841–1853, DOI 10.5194/nhess-16-1841-2016, URL https://nhess.copernicus.org/articles/16/1841/2016/

Wahl T, Haigh ID, Nicholls RJ, et al (2017) Understanding extreme sea levels for broad-scale coastal impact and adaptation analysis. Nature Communications 8(May):16,075, DOI 10.1038/ncomms16075

Walsh KJE, McBride JL, Klotzbach PJ, et al (2016) Tropical cyclones and climate change. WIREs Climate Change 7(1):65–89, DOI 10.1002/wcc.371, URL http://onlinelibrary.wiley.com/doi/abs/10.1002/wcc.371, _eprint: https://onlinelibrary.wiley.com/doi/pdf/10.1002/wcc.371

Wilkinson MD, Dumontier M, Aalbersberg IJ, et al (2016) The FAIR Guiding Principles for scientific data management and stewardship. Scientific Data 3(1):160,018, DOI 10.1038/sdata.2016.18, URL http://www.nature.com/articles/sdata201618

Wolff C, Vafeidis AT, Lincke D, Marasmi C, Hinkel J (2016) Effects of scale and input data on assessing the future impacts of coastal flooding: An application of diva for the emilia-romagna coast. Frontiers in Marine Science 3:41, DOI 10.3389/fmars.2016.00041

Woodworth PL, Hunter JR, Marcos M, et al (2016) Towards a global higher-frequency sea level dataset. Geoscience Data Journal 3(2):50–59, DOI 10.1002/gdj3.42

Xian S, Yin J, Lin N, Oppenheimer M (2018) Influence of risk factors and past events on flood resilience in coastal megacities: Comparative analysis of NYC and Shanghai. Science of the Total Environment 610-611:1251–1261, DOI 10.1016/j.scitotenv.2017.07.229

Yamazaki D, Ikeshima D, Tawatari R, et al (2017) A high-accuracy map of global terrain elevations. Geophysical Research Letters 44(11):5844–5853, DOI 10.1002/2017GL072874, URL https://agupubs.onlinelibrary.wiley.com/doi/abs/10.1002/2017GL072874, _eprint: https://agupubs.onlinelibrary.wiley.com/doi/pdf/10.1002/2017GL072874

Yesudian AN, Dawson RJ (2021) Global analysis of sea level rise risk to airports. Climate Risk Management 31:100,266, DOI 10.1016/j.crm.2020.100266

Supplementary Information

S-1 Supporting Information

In this study, we use a simple inundation model with a new global elevation dataset (Kulp and Strauss, 2018, 2019) to highlight the limitations and consequences of using extreme sea level (ESL) metrics that only consider the physical heights of water levels, specifically ESL AFs (frequency and return level) and ESL hazard allowances. We connect ESLs measured at a global network of tide gauges to present-day population exposure for 414 coastal cities around the world. We project future changes in both the frequency and return levels of historical ESLs and the exposure of current populations under two climate change scenarios (Sec. S-1.2). We note that these are not estimates of future population exposure because we do not make future projections of population change. Additionally, we use a simple, static inundation approach that has not been globally validated. These projections are merely intended to highlight the limitations of physical ESL metrics when quantifying coastal flood risk. The performance of our inundation modeling approach has not been extensively validated and is challenged by a lack of observed flood extents for which to validate our model. Sophisticated flood risk analyses are needed to better understand current and future risk levels.

An overview of the sources of information used to generate population inundation estimates are given in Fig. S-1. First, we estimate the present-day probability of ESLs of various heights at a global network of tide gauges using extreme value theory and a long-term record of hourly sea level observations (Sec. S-1.1). Second, we project changes in both the frequency and height of ESLs using local probabilistic projections of relative sea level change (RSLC)[3] that incorporate ice sheet mass loss estimates from structured expert judgment (Sec. S-1.2). Third, we produce 1-dimensional, city-specific functions of population versus ground elevation to estimate the current population exposure to ESLs (Sec. S-1.3). Fourth, by combining the population exposure damage functions with the future estimates of ESLs, we compute the change in the number of people exposed to various ESLs for each city using population exposure AFs (Sec. S-1.4).

S-1.1 Estimating extreme sea levels

S-1.1.1 Tide gauge data

We use long-term records of hourly or sub-hourly sea level observations from quality controlled tide gauges from the University of Hawaii Sea Level Center[4] and also supplement with other tide gauges from the GESLA2 data set (Woodworth et al, 2016). We limit our use of tide gauge records to only those that have record lengths >30 consecutive years in which each year has >80 percent of observations available. In total, we use 360 unique tide gauges, with median and average record lengths of 48 and ∼54 years, respectively (a list of the tide gauges used is given in the supporting information). We estimate the daily maximum sea level for each day in the tide gauge record with > 80 percent of available observations. We note that this temporal resolution only facilitates the estimation of still-water heights. Tide gauges are often placed inside protected harbors. This generally prevents capturing wave setup effects and swash. Wave setup is more likely to be picked up at tide gauges where there are shallow sloping beaches. Moreover, the time averaging of the observations also filters out contributions from waves, which can be significant contributors to extremes (Melet et al, 2018; Arns et al, 2017). To isolate the variation in extreme sea levels (ESLs), we remove the effect of mean sea level (MSL) change by subtracting the annual MSL from each daily maximum value (i.e., values are de-trended). The de-trended daily maximum tide values are then referenced to local mean higher high water (MHHW; relative to the de-trended mean sea level), defined as the average highest high tide at the tide gauge over a given period (here, either 1993–2012 or the last available 19-year period in the record). The local tidal component is not removed.

[3] Relative sea level change is defined as the change in local mean sea level relative to the sea floor or the underwater surface of the solid Earth (Gregory et al, 2019).

[4] retrieved from: https://uhslc.soest.hawaii.edu, January 2020; (Caldwell et al, 2015)

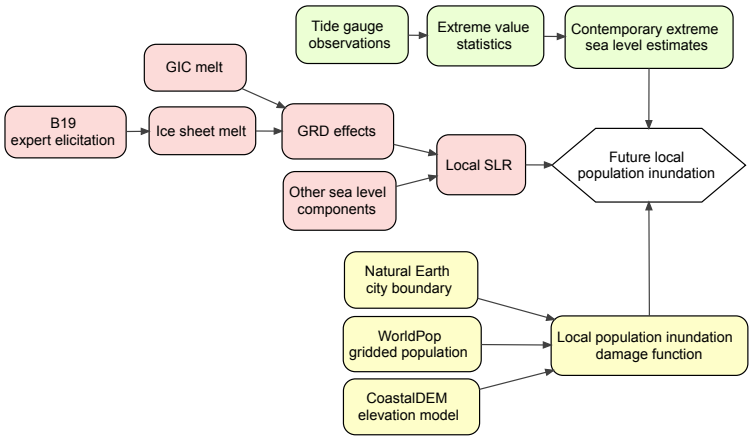

Fig. S-1: Flow of information used in this study to produce projected local population exposure estimates (white hexagon). Green rectangles are for extreme sea level estimation. Red rectangles are for sea-level rise projections. Yellow rectangles are for local population exposure estimates. B19 is Bamber et al (2019); SLR is sea-level rise; GIC are glaciers and ice caps; GRD are gravitational, rotational, and deformational effects; "Other sea level components" includes land water storage, oceanographic processes, and non-climatic background changes, such as glacial-isostatic adjustment.

S-1.1.2 Modeling the probability of rare events with extreme value theory

Extreme value theory is commonly used to produce models that describe unusual or rare behavior (Coles, 2001b; Embrechts et al, 1997). If a modeled fit is considered "good", it can be used to extrapolate the frequency of events of interest, sometimes well beyond the length of the observation record (e.g., determining the height of 100-yr ESL event from a 30-yr record of tide gauge data). Various extreme value distributions and approaches to implement them have been proposed (Coles, 2001b; Embrechts et al, 1997), but in the case of ESL estimation, there currently is not an agreed upon "best approach". Depending on the specific project goals, a particular extreme value modeling strategy may be preferred over another. Following previous studies (Tebaldi et al, 2012; Buchanan et al, 2017; Rasmussen et al, 2018; Frederikse et al, 2020; Wahl et al, 2017), we the extreme values at each tide gauge using a generalized Pareto distribution (GPD; Pickens, 1975; Coles, 2001c,a).

The GPD is a peaks over threshold extreme value modeling approach that describes the probability of a given ESL height conditional on the exceedance of a threshold. The GPD has the advantage over other generalized extreme value (GEV) models for two reasons. First, if the tide gauge record is short, a peaks over threshold approach that uses sub-annual observations/extremes may be preferred over other generalized extreme value (GEV) models that only use annual maxima (i.e., one value per year; Lang et al, 1999; Cunnane, 1973). In other words, more information is retained in the peaks over threshold approach. Using annual maxima can waste data since a year of observations is being represented with a single value. For some locations, more than half of the highest observed ESLs have occurred within the same year (e.g., Boston, U.S.A.; Baranes et al, 2020). Furthermore, if a single annual maxima coincides with a low tidal level, the tidal influence is ignored despite its relevance to estimating ESLs. Second, unlike other GEV distributions (such as the Gumbel; Buchanan et al, 2017), the GPD includes a parameter that allows for the flexibility for the distribution to take on different shapes (shape parameter, ξ, and its value depends on the characteristics of the underlying data), and 3) it can be combined with a Poisson rate parameter to translate ESL exceedance probabilities into expected numbers of annual ESL exceedances (the assumption being that GPD exceedances

are Poisson distributed). The latter may be more intuitive and thus better for communicating the frequency of ESL events.

Following (Coles, 2001a), the cumulative distribution function of the GPD is given by:

$$G(z|u,\alpha,\xi) = \Pr(Z \leq z | Z \geq u) = \begin{cases} 1 - \left(1 + \xi \frac{(z-u)}{\alpha}\right)^{-1/\xi} & \text{for } \xi \neq 0, \\ 1 - \exp\left(-\frac{(z-u)}{\alpha}\right) & \text{for } \xi = 0, \end{cases} \tag{S-1}$$

with $u \in \mathbb{R}$, $\xi \in \mathbb{R}$, and valid for $\alpha > 0$, $z \geq u$ when $\xi \geq 0$ and $u \geq z \geq u - \alpha/\xi$ when $\xi < 0$. The parameters are as follows, ξ is the shape parameter, α is the scale parameter, and u is the threshold water-level above which return levels are estimated with the GPD.

Selecting the GPD threshold u (sometimes called the "location" parameter–not to be confused with geographic location) is critical element of the peaks over threshold approach as it can have substantial influence on the tail extrapolation. If the threshold is too low, it could bias the estimates because the included values may not be extreme enough. On the other hand, if the threshold is too high, the variance might be too large because too few points are being included in the analysis (Lang et al, 1999). The selection of the threshold can influence the parameter estimation (Coles and Tawn, 1996; Coles and Powell, 1996). GPD thresholds are often chosen either graphically, by looking at a mean excess plot (Embrechts et al, 1997), or by simply setting it to some high percentile of the data (DuMouchel, 1983). The graphical approach is infeasible in this study's case because we are working with several hundred tide gauges. Instead, we set the GPD threshold at the 99th percentile for all sites. The 99th percentile is generally is above the highest seasonal high tide, balances the bias-variance trade-off in the GPD parameter estimation (Tebaldi et al, 2012) and has been found to perform well at global scales (Wahl et al, 2017). Because of the subjective nature of choosing the GPD threshold (Davison and Smith, 1990; Coles and Tawn, 1994), an automated approach remains elusive (Dupuis, 1998; MacDonald et al, 2011).

After the GPD threshold is selected, the daily maximum sea levels above u are de-clustered to satisfy the statistical independence assumption of the GPD. More specifically, the largest daily maximum sea level value within 3 days of each GPD exceedance is used. The remaining GPD parameters are then estimated using maximum likelihood, and their uncertainty is calculated from their estimated covariance matrix. To account for uncertainty in the GPD fit, the estimated covariance matrix is later sampled using a Latin hypercube sampling to produce 1000 normally distributed GPD parameter pairs. Note that the fit of the GPD and the uncertainty bounds may not always well capture the observed exceedances (e.g., San Juan; Fig 1A). While we extrapolate estimates for ESL events up to the frequency of the 1000-yr event, we caution in using any estimate of ESL that exceeds four times the length of the observation record (Pugh and Woodworth, 2014).

The scale, shape, and threshold/location GPD parameters reflect the historical experience with meteorological and oceanographic phenomena that drive ESL events (Pugh and Woodworth, 2014; Coles, 2001c,a; Tebaldi et al, 2012). The shape parameter governs the concavity and upward statistical limit of $G(z)$. Positive shape parameters are indicative of sites exposed to strong tropical cyclones and/or a wide continental shelf that increases storm surge potential (e.g., sites along eastern North America), while negative shape parameters are associated with weaker, infrequent storms, and potentially a narrower continental shelf (e.g., sites in Western North and South America, Fig. S-2A). ESL frequency distributions with $\xi > 0$ are "heavy tailed" and concave up, due to a larger variation in extremes (e.g., existence of tropical and extra-tropical cyclones). Distributions with $\xi < 0$ are "thin tailed", concave down, and have a statistical upper bound on ESLs. The scale parameter α reflects the variability in the distribution of threshold exceedances (i.e., the width of the distribution). The largest scale parameters are found in regions with frequent wintertime extratropical cyclone activity (e.g., the North Sea and Gulf of Alaska; Fig S-2B). The GPD threshold exceedances are shown in Fig. S-2C. The GPD parameters are given in the supporting data files.

S-1.1.3 Mixture normal-extreme value theory probability model

Because the GPD only is defined above the threshold u, an additional distribution is needed to characterize events below u. Following MacDonald et al (2011) and Ghanbari et al (2019), we implement a non-stationary probability mixture model (Eq. S-1.1.3) that simultaneously characterizes the bulk and upper tail of the de-trended daily maximum tide gauge data. The bulk of the data follows a Normal distribution and is fitted as such, however, the upper tail of is not (Fig. S-3. As such, it is considered separately, and a GPD is fit to the

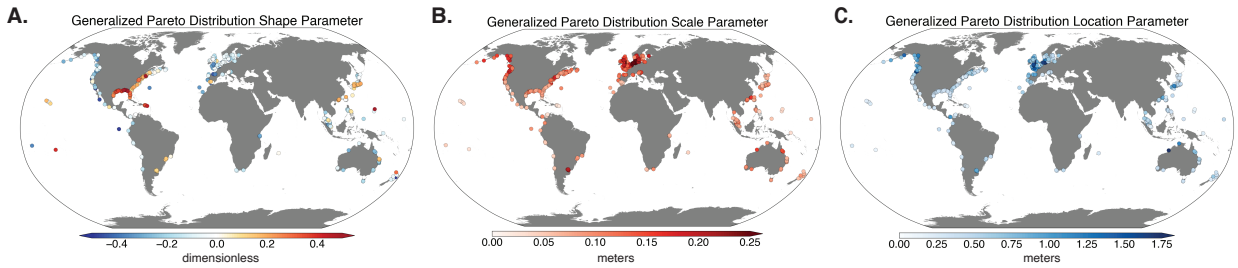

Fig. S-2: **A.** A global map showing the generalized Pareto distribution (GPD) shape parameter (ξ; dimensionless) at cities around the world. **B.** As for A, but for the GPD scale parameter (α; meters above mean higher high water). **C.** As for A, but for the GPD threshold or "location" parameter (u; meters above mean higher high water).

observed extreme values. Studies often ignore the bulk portion of the ESLs distribution, or assume it is well fitted by an arbitrary distribution without empirically testing such fits (e.g., a Gumbel, see Buchanan et al, 2016; Buchanan et al, 2017; Rasmussen et al, 2018, 2020). These are critical assumptions because changes in the most frequent ESLs are the most sensitive to changes in MSL (Buchanan et al, 2017), therefore the increase in the frequency of frequent ESL will be experienced soonest.

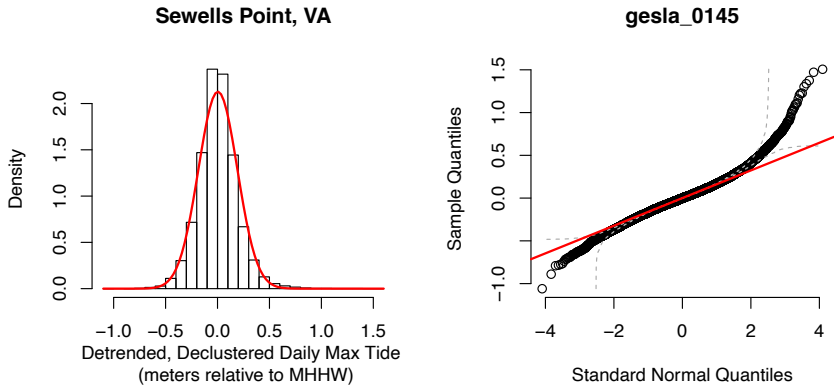

Fig. S-3: **Left:** A histogram of observed maximum daily water levels for Sewell's Point, VA (USA) and a Normal distribution fit (red line). **Right:** As for Left, but a quantile-quantile plot. Note that the bulk of the maximum daily water levels fits a Normal distribution, but the tails do not.

The cumulative distribution function of the mixture model is given by:

$$F(z|\mu,\sigma,u,\alpha,\xi,\varphi) = \begin{cases} (1-\varphi)\,\frac{\mathcal{N}(z|\mu,\sigma)}{\mathcal{N}(u|\mu,\sigma)} & \text{if } z < u, \\ (1-\varphi) + \varphi G(z|u,\alpha,\xi) & \text{if } z \geq u \end{cases} \tag{S-2}$$

where $\mathcal{N}(z|\mu,\sigma)$ and $G(z|u,\alpha,\xi)$ are the Normal and conditional GPD cumulative distribution functions, respectively, and φ is the ratio of de-clustered daily maximum sea level observations that meet or exceed u over the total number of observations. The Normal distribution parameters μ and σ are estimated from the de-trended daily maximum sea level observations, and u is the GPD threshold. An additional benefit of the Normal-GPD probability mixture model (Eq. S-1.1.3) is that it somewhat bypasses the uncertainty in the GPD threshold choice of u through the use of a smooth transition function between the bulk and tail components (MacDonald et al, 2011; Behrens et al, 2004).

To account for local change in mean sea level (described below), the GPD threshold u and the Normal distribution parameter μ linearly shifts. We do not consider future changes in storm frequency (Walsh et al,

2016), intensity (Sobel et al, 2016), or track (Garner et al, 2017), which could all modify these statistical parameters. We also do not consider changes in the tide-surge interaction (Schindelegger et al, 2018; Arns et al, 2017), the surge-sea level interaction (Little et al, 2015), or changes in geomorphology (Familkhalili and Talke, 2016; Talke et al, 2014), all of which may impact future ESL estimates.

For a given tide gauge, the annual expected number of exceedances of height z are given by the Normal-GPD model as follows:

$$N(z) = \begin{cases} n_y \left(1 - \left[\frac{(1-\varphi)}{1+\mathrm{erf}\left(\frac{u-\mu}{\sigma\sqrt{2}}\right)} \left(1 + \mathrm{erf}\left(\frac{z-\mu}{\sigma\sqrt{2}}\right)\right)\right]\right) & \text{if } z < u, \\ n_y \varphi \left(1 + \frac{\xi(z-\mu)}{\sigma}\right)^{-\frac{1}{\xi}} & \text{if } z \geq u, \xi \neq 0 \\ n_y \varphi \exp(-\frac{z-\mu}{\sigma}) & \text{if } z \geq u, \xi = 0 \end{cases} \tag{S-3}$$

where n_y is the number of observations per year and $\mathrm{erf}(\cdot)$ is the error function. The exceedances are assumed to follow a Poisson process, with a mean of $n_y \times \varphi$.

S-1.2 Relative sea level change projections

Probabilistic, time-varying, local relative sea level change (RSLC) projections for each tide gauge are taken from the component-based study of Kopp et al (2014), except that ice sheet contributions are from the structured expert judgement (SEJ) study of Bamber et al (2019). Projections of RSLC after mid-century are highly dependent on ice sheet melt because of their potential for substantial contributions to global mean sea-level rise (Oppenheimer et al, 2019; Kopp et al, 2019). However, incomplete understanding of the physical processes that govern ice sheet melt inhibits realistic representations in process-based models. In such cases of incomplete scientific understanding, SEJ using calibrated expert responses is one approach for estimating such uncertain quantities (as employed here). Each RSLC probability distribution is conditional on a scenario in which global mean surface air temperature (GSAT) stabilizes in 2100 at either +2 °C (consistent with the Paris Agreement; UNFCCC, 2015) or +5 °C (consistent with unchecked emissions growth; GSAT relative to 1850–1900; Hausfather and Peters, 2020). Samples from each RSLC probability distribution are used to shift the ESL return curves in the direction of the RSLC. Fig. 1A shows the future (2070) ESL return curve for a tide gauge located in San Juan (Puerto Rico). The "kinks" in the return curves appear as a result of the highest samples in the RSLC probability distribution causing the expected ESL frequency calculation to saturate and then subsequently increase the expected number of ESL events. Both the positioning and the presence of the kinks in the return curves are sensitive to the choice of where the upper-tail of the RSLC distribution is truncated (Rasmussen et al, 2020).

The other RSLC component contributions are from ocean thermal expansion, glaciers and ice caps, and land-water storage. General circulation model (GCM) output is used to generate the steric and glacial ice melt sea level components for each global mean surface air temperature (GSAT) stabilization scenario. The +2 °C scenario used the GCM outputs specified for the same GSAT scenario in Rasmussen et al (2018) and the +5 °C scenario used GCM outputs from the representative concentration pathway (RCP) 8.5 from Kopp et al (2014). Also accounted for are regional effects such as ocean dynamics (from GCM output), gravitational and rotational effects of ice mass redistribution, glacial isostatic adjustment, and other local vertical land motion factors (e.g., tectonic uplift, sediment compaction and ground water withdrawal). Probability distributions of local RSLC are produced using 10,000 Latin hypercube samples of each individual sea level component contribution. The probability distributions are truncated at the 99.9th percentile to remove samples that are deemed to be physically implausible (Oppenheimer et al, 2019). As noted by Rasmussen et al (2020), both ESL frequencies and allowances are sensitive to truncation selection. More details and limitations to the RSLC projections are provided elsewhere (Kopp et al, 2014; Bamber et al, 2019; Rasmussen et al, 2020).

S-1.3 Exposure analysis

The vertical population profile of a city can determine the population exposure to a given ESL event. We produce 1-dimensional (vertical) population profiles for 414 global cities using CoastalDEM and population density data from the WorldPop 2010 high resolution (3 arc second) gridded global population data set (Tatem, 2017). In order to simplify our analysis and also isolate the impact of RSLC on population exposure, we assume that population remains fixed in time. Thus, our results are not literal projections of future population exposure—which will depend upon population growth (Hauer et al, 2016; Jongman et al, 2012) and the dynamic response of the population to RSLC (Merkens et al, 2016; Hauer, 2017)—but are instead intended to highlight the impact of ESL events relative to changes in their frequency. A population exposure profile for San Juan (Puerto Rico) is given in Fig. 1B. Exposure profiles for all cities are included in the supporting data.

We map flood extents for each city using the "bathtub" model, a static inundation approach that only considers the vertical elevation of two surfaces, 1) the terrain and 2) a given ESL return level (e.g., 100-yr event) measured at the nearest tide gauge within a 100-km radius of each city center. The return level of interest is spatially extrapolated over the terrain. Static inundation approaches have many limitations, including overestimating observed flood extents relative to hydrodynamic models (Breilh et al, 2013; Gallien, 2016; Ramirez et al, 2016; Seenath et al, 2016; Bates et al, 2005; Vousdoukas et al, 2016). However, hydrodynamic modeling is computationally expensive, and producing state-of-the-art projections of population exposure is not the goal of this analysis. Land elevation data are from CoastalDEM, a modified version of NASA's Shuttle Radar Topography Mission (SRTM) digital elevation model (DEM) that uses a neural network trained using lidar-derived elevation data in the U.S. (NOAA, 2020) to reduce SRTM errors (Kulp and Strauss, 2018, 2019; Farr et al, 2007). The SRTM is a near-global DEM commonly used for flood exposure modeling but is known to have large vertical bias (an estimated 3.7 m in coastal areas in the U.S.; Kulp and Strauss, 2018). This is important because coastal flood risk analysis is largely performed within this elevation range and these biases are roughly the same magnitude as projections of future local RSLC over this century (generally < 2 m relative to 2000; Oppenheimer et al, 2019; Gesch, 2018). More details and limitations are provided in Kulp and Strauss (2018, 2019).

Most populations living in low-lying areas around the world (e.g., deltaic regions) are very likely protected by flood defenses such as levees, seawalls, and deliberately raised structures (e.g., buildings on stilts; Scussolini et al, 2016). Following previous flood exposure studies (Neumann et al, 2015; Hanson et al, 2011; Kulp and Strauss, 2019; McGranahan et al, 2007; Jongman et al, 2012; Lichter et al, 2011), our exposure estimates do not account for these defenses because they can be overtopped and breached; only the population in the floodplain is considered. However, protection is assumed to only change the flood hazard and enters our integrated calculations of population exposure that consider all ESL return levels (Sec. S-1.1). To our knowledge, verified, location-specific levels of protection are not available at the global scale[5]. To account for flood defenses that provide a margin of safety, we make multiple arbitrary assumptions regarding the current level of protection for all cities. Specifically, we produce results assuming spatially uniform "no protection" and protection up to the height of the 1- and 10-yr ESL event. These assumptions may greatly differ from reality and could lead to gross over-estimates for cities with existing flood protection that afford a high margin of safety from rare storms, such as London, New Orleans, Tokyo, Shanghai, and most major cities in the Netherlands (Nicholls et al, 2008; Hallegatte et al, 2013; Xian et al, 2018; Scussolini et al, 2016). Despite this, we still include protection assumptions for all cities to 1) limit the inclusion of the lowest elevations which are most prone to vertical errors in the DEM and 2) to highlight the importance of the flood protection assumption and the need for accurate estimates thereof (e.g., Scussolini et al, 2016). The protection assumptions do not impact AFs above the height of the protection level, but can significantly impact integrated metrics that consider all ESLs and impacts, such as the expected annual exposure (EAE; Table S-4)(Kulp and Strauss, 2017).

A vertical adjustment was made to the ESLs to reference the same local mean higher high water (MHHW) datum as CoastalDEM. ESLs use tide gauge data for estimating MHHW, while CoastalDEM uses the glob-

[5] However, Hallegatte et al (2013) and Scussolini et al (2016) give upper and lower estimates of flood protection for over 100 major cities around the world based on surveyed responses from local experts. But these responses have not been verified, and local protection can vary within a city.

ally extensive MSL model MSS CNES-CLS15[6], based on a 1993—2012 record of satellite sea surface height measurements from TOPEX/Poseidon, and MHHW deviations from MSL provided by Mark Merrifield, University of Hawaii, developed using the model TPX08 (Egbert and Erofeeva, 2002). Using the National Oceanic and Atmospheric Administration's (NOAA) VDatum tool (version 3.7; Parker et al, 2003), we convert these measurements to vertically reference EGM96, and we subtract the resulting surface from CoastalDEM to convert its vertical datum to MHHW (adjustments are provided in the supporting data files).

We take a static inundation modeling approach by spatially extrapolating return periods of ESLs, measured at tide gauges, onto the surrounding topography. We map one tide gauge to each city. For cities where there is more than one tide gauge within a 100-km radius (e.g., Willet's Point and the Battery in NYC), the tide gauge with the longest record is used (the tide gauges assigned to each city are listed in the supporting data files). While the height of a given ESL return period may vary within a city, in part due to complicated bathymetry and coastlines, Kulp and Strauss (2017) has shown that ESL population exposure results for the U.S. are generally insensitive to tide gauge assignment within a 100-km radius. In any case, static inundation approaches do not account for complex local geomorphology, local ocean dynamics, and frictional losses as water moves over different land surfaces (e.g., wetlands, beaches, urban areas). More complex hydrodynamic inundation approaches that model the flow of the ocean onto a variety of land surfaces could be used to more accurately estimate local floods for cities across the globe. However, such an approach is out of the scope of this study as our intention is to merely highlight the limitations of physical ESL metrics. Furthermore, we note that hydrodynamic inundation modeling may not necessarily outperform simpler approaches, especially in active tropical cyclone regions (Hunter et al, 2017; Muis et al, 2016, 2017; Wahl et al, 2017), in part due to poor representation of tide-surge interactions (Arns et al, 2020) and short simulation periods that are less likely to produce rare, extreme events found in multi-decadal tide gauge records. For some locations, the height of the 100-yr ESL event can be under-predicted by up to 3 meters compared to tide gauge-derived estimates (supporting information of Muis et al, 2017).

The WorldPop population data are resampled to align with CoastalDEM raster (for more details, see Kulp and Strauss, 2019), integrated over select elevations (-2 to 13 m above MHHW, either 0.25 or 0.5 m increments), and then tabulated according to the satellite-derived urban footprint for each city from Natural Earth (which may differ from the actual administrative boundary; Kelso and Patterson, 2012). We note that Kulp and Strauss (2019) instead uses LandScan population density at 30 arc seconds. Coastal cities are only included in the analysis if there are populations with in the defined boundary at any elevation < 13 m above local MHHW. Connected components analysis excludes low-elevation inland areas that are not linked to the ocean. Linear interpolation is used between each select elevation to produce a continuous 1-dimensional population exposure profile $D(z)$, where z is the ESL height. We note that z could be a vector to account for spatial differences in ESL height for the same return period within a city and also spatial variation in flood protection.

Exposure analyses are most sensitive to spatially-autocorrelated vertical errors in the DEM at local scales and when assessing population vulnerability at low elevations (e.g., < 0.5 m; Kulp and Strauss, 2019). The higher the elevation that population exposure is being assessed at (e.g., longer return periods, such as the 100-yr event), the less of an impact these errors will have on exposure (Kulp and Strauss, 2019). To assess the impact of elevation errors on population exposure AFs, we use the example of the 100-year ESL event in New York City. Considering lidar topography as ground truth, we find that the EAE AFs are generally insensitive to errors in CoastalDEM; small differences only appear by 2100 for the +5 °C scenario (2.3 vs 2.6; Table S-2). This is despite CoastalDEM underestimating population exposure relative to lidar (connected components analysis not performed for this test; Tables S-1,S-2). We note that CoastalDEM was trained on lidar elevation data in the U.S., so locations outside the U.S. may be more sensitive.

[6] Aviso. MSS CNES-CLS15, https://www.aviso.altimetry.fr/en/data/products/auxiliary-products/mss.html (2015)

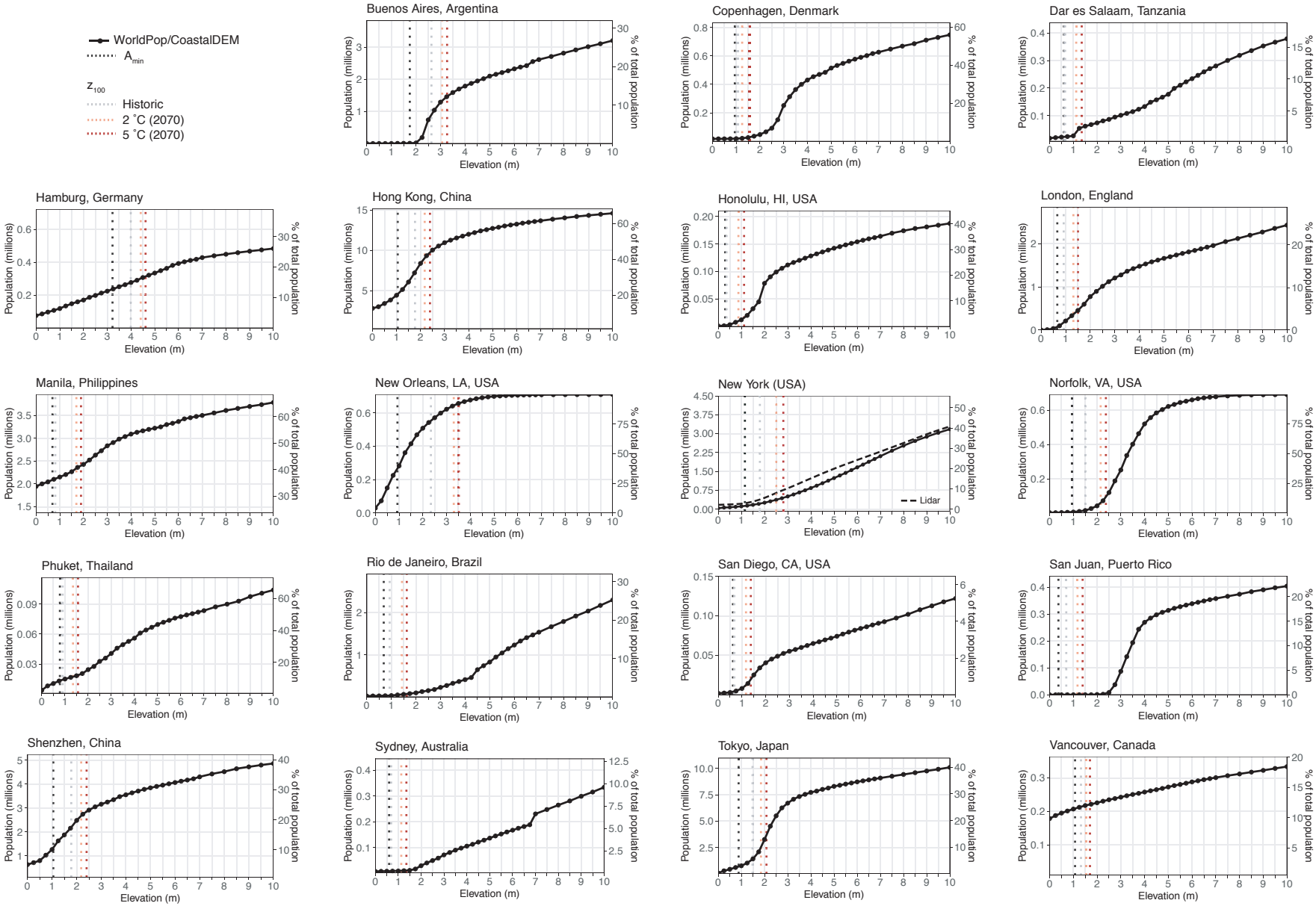

Fig. S-4: Population exposure functions that estimate the total population currently exposed to flooding as a function of ESL height (meters above MHHW) for cities given in Table 1. Filled black circles are population data from the 2010 WorldPop global population database (Tatem, 2017) applied to the elevation surfaces of CoastalDEM (Kulp and Strauss, 2018, 2019). Linear interpolation is used to produce a continuous curve between the WorldPop data (black line). City boundaries are those as defined by Kelso and Patterson (2012) and may differ from actual political boundaries. Populations are assumed to remain constant in time. Denoted is the current level of protection (A_{min}), assumed to be the 10-yr ESL event, the height of the historical 100-yr ESL event (grey), and the expected heights of the 100-yr ESL event under a +2 °C (orange) and +5 °C (red) climate scenario. Also shown for New York City is a population profile generated using a 0.3-m horizontal resolution light detection and ranging (LiDAR)-derived digital elevation model for the City of New York (https://data.cityofnewyork.us/City-Government/1-foot-Digital-Elevation-Model-DEM-/dpc8-z3jc).

S-1.4 Estimating physical and population exposure amplification factors

Following Buchanan et al (2017), the ESL frequency AF for an event of height z^* under uncertain RSLC is $\mathbb{E}[N(z^* - \delta)/N(z^*)]$, where $N(z^* - \delta)$ is the expected number of exceedances of height z^* after considering RSLC δ (Sec. S-1.1). The ESL return level AF is given by $1 + \mathbb{E}[\delta]/z^*$. Here, we extend the ESL return level AF to changes in population exposure. We define the population exposure AF for an event of height z^* under uncertain RSLC as $\mathbb{E}[D(z^* + \delta)/D(z^*)]$, where $D(\cdot)$ is a 1-dimensional vertical population profile of a city (Sec. S-1.3). Note that since $D(\cdot)$ is solely a function of z, the frequency amplification of population exposure events is equivalent to the ESL frequency AFs for the same city. Probability distributions of ESL AFs (frequency and return level) and population exposure AFs are produced for each tide gauge using the RSLC samples for each climate scenario (Sec. S-1.2). Results are then taken from these distributions.

2.0 °C	2010	2070		2100	
	Population (thousands)	Population (thousands)	Pop Exposure AF	Population (thousands)	Pop Exposure AF
Lidar	399 (293-564)	607 (488-745)	1.5 (1.2-1.9)	708 (518-938)	1.8 (1.3-2.4)
CoastalDEM	229 (168-324)	351 (280-440)	1.5 (1.2-1.9)	421 (297-596)	1.8 (1.3-2.6)

Table S-1: Estimated total population exposure and amplification factors for the 100-yr extreme sea level (ESL) event for New York City using 1) a 0.3-m horizontal resolution light detection and ranging (LiDAR)-derived digital elevation model for the City of New York (https://data.cityofnewyork.us/City-Government/1-foot-Digital-Elevation-Model-DEM-/dpc8-z3jc) and 2) CoastalDEM. Future projections assume a climate scenarios in which global mean surface air temperature is stabilized in 2100 at +2 °C (relative to 1850–1900; Bamber et al, 2019).

5.0 °C	2010	2070		2100	
	Population (thousands)	Population (thousands)	Pop Exposure AF	Population (thousands)	Pop Exposure AF
Lidar	399 (293-564)	687 (529-880)	1.7 (1.3-2.2)	917 (617-1,398)	2.3 (1.5-3.5)
CoastalDEM	229 (168-324)	405 (303-548)	1.8 (1.3-2.4)	589 (355-1,010)	2.6 (1.6-4.4)

Table S-2: As for Table S-1, but for a climate scenarios in which global mean surface air temperature is stabilized in 2100 at +5 °C (relative to 1850–1900; Bamber et al, 2019).

100-yr ESL event			2070 (5.0 °C)					
	Historical		Physical metrics			Societal metrics		
City (Total population in thousands)	100-yr ESL (m)	% Pop exposed	RSLC (m)	ESL frequency AF	ESL level AF	Pop exposure AF	Pop exposed (thousands)	% Pop exposed
Buenos Aires, Argentina (11,980)	2.6 (2.1-3.2)	7.5%	0.6 (0.3-1.1)	8 (2-20)	1.2 (1.1-1.4)	1.7 (1.4-1.9)	1,520 (1,241-1,682)	12.7% (10.4-14.0%)
Copenhagen, Denmark (1,337)	1.1 (1.0-1.1)	1.5%	0.5 (0.1-1.0)	841 (10-5575)	1.5 (1.1-1.9)	3.1 (1.1-2.5)	62 (21-51)	4.7% (1.6-3.8%)
Dar es Salaam, Tanzania (2,322)	0.7 (0.6-0.7)	1.0%	0.7 (0.3-1.2)	4720 (620-6678)	2.1 (1.5-2.9)	3.7 (1.1-3.1)	83 (26-70)	3.6% (1.1-3.0%)
Hamburg, Germany (1,854)	4.0 (3.6-4.4)	14.9%	0.6 (0.3-1.1)	9 (2-22)	1.2 (1.1-1.3)	1.2 (1.1-1.2)	321 (293-338)	17.3% (15.8-18.2%)
Hong Kong, China (22,232)	1.8 (1.2-2.6)	32.9%	0.6 (0.2-1.2)	120 (2-155)	1.4 (1.1-1.7)	1.4 (1.2-1.5)	10,334 (8,437-10,847)	46.5% (38.0-48.8%)
Honolulu, HI, USA (466)	0.4 (0.3-0.4)	0.5%	0.8 (0.4-1.3)	14017 (14455-14455)	3.1 (2.0-4.7)	41.2 (3.2-18.4)	96 (7-43)	20.5% (1.6-9.1%)
London, England (9,878)	0.9 (0.7-1.1)	1.8%	0.6 (0.3-1.0)	223 (12-1242)	1.6 (1.3-2.1)	4.2 (1.8-4.1)	750 (310-728)	7.6% (3.1-7.4%)
Manila, Philippines (5,782)	0.8 (0.7-0.9)	36.6%	1.1 (0.7-1.6)	17424 (7870–*)	2.3 (1.9-3.0)	1.3 (1.1-1.2)	2,757 (2,280-2,601)	47.7% (39.4-45.0%)
New Orleans, LA, USA (711)	2.4 (1.2-4.3)	77.9%	1.2 (0.8-1.7)	90 (3-26)	1.5 (1.4-1.7)	1.2 (1.1-1.2)	661 (635-678)	92.9% (89.3-95.3%)
New York, NY, USA (12,520)	1.9 (1.5-2.3)	3.7%	0.8 (0.4-1.3)	228 (3-296)	1.4 (1.2-1.7)	1.8 (1.2-2.1)	837 (578-957)	6.7% (4.6-7.6%)
Norfolk, VA, USA (695)	1.5 (1.1-2.0)	2.3%	0.9 (0.5-1.4)	343 (7-1660)	1.6 (1.3-1.9)	10.7 (2.7-13.9)	169 (42-219)	24.3% (6.1-31.5%)
Phuket, Thailand (159)	0.9 (0.8-1.0)	9.0%	0.7 (0.3-1.2)	6012 (208–*)	1.7 (1.3-2.3)	2.3 (1.1-1.8)	33 (16-26)	20.8% (10.3-16.1%)
Rio de Janeiro, Brazil (9,110)	0.9 (0.8-1.1)	0.3%	0.7 (0.3-1.2)	3951 (30-14619)	1.7 (1.4-2.3)	4.1 (1.5-3.5)	129 (49-110)	1.4% (0.5-1.2%)
San Diego, CA, USA (2,323)	0.7 (0.7-0.7)	0.2%	0.7 (0.3-1.2)	9611 (798-15431)	2.0 (1.5-2.8)	11.0 (2.0-8.6)	48 (9-38)	2.1% (0.4-1.6%)
San Juan, Puerto Rico (1,821)	0.7 (0.5-1.1)	0.0%	0.7 (0.3-1.2)	10597 (11–*)	2.0 (1.5-2.7)	16.3 (1.2-5.3)	2 (<1-1)	0.1% (<0.1- <0.1%)
Shenzhen, China (12,518)	1.8 (1.2-2.6)	17.4%	0.6 (0.2-1.2)	120 (2-155)	1.4 (1.1-1.7)	1.4 (1.1-1.4)	2,993 (2,496-3,131)	23.9% (19.9-25.0%)
Sydney, Australia (3,483)	0.7 (0.6-0.7)	0.2%	0.7 (0.3-1.1)	8942 (374-16480)	2.0 (1.5-2.7)	4.8 (1.1-2.6)	39 (9-21)	1.1% (0.3-0.6%)
Tokyo, Japan (25,339)	1.5 (1.0-2.1)	5.5%	0.6 (0.2-1.2)	435 (2-830)	1.4 (1.1-1.8)	3.8 (1.4-4.2)	5,357 (1,907-5,965)	21.1% (7.5-23.5%)
Vancouver, Canada (1,810)	1.3 (1.1-1.6)	11.8%	0.4 (0.1-0.9)	436 (2-1065)	1.3 (1.0-1.6)	1.1 (1.0-1.1)	232 (215-229)	12.8% (11.9-12.7%)

Table S-3: Table listing both physical and societal extreme sea level (ESL) metrics for select major coastal cities. Given are the heights of the historical 100-yr ESL return period (meters relative to mean higher high water; expected/5th/95th percentile), the percent of the total population exposed to the expected 100-yr ESL event, 2070 probabilistic relative sea-level change (RSLC) (meters, relative to 1991–2009) from a climate scenario in which global mean surface air temperature (GSAT) is stabilized in 2100 at +5 °C (relative to 1850–1900; Bamber et al, 2019), ESL return period amplification factors (AFs) for the 100-yr ESL event, ESL return level AFs for the 100-yr ESL event, the population exposure AF, the estimated total population exposed to the future 100-yr ESL event (thousands), and the same number as a percent of the total population. The expected value and the 5/95 percentile of the estimate are given for each. The 5/95 percentile for the current ESL return period considers the uncertainty in the generalized Pareto distribution (GPD) parameters, while the 5/95 percentile for RSLC and AFs reflect the uncertainty from both contributions to local RSLC and from the GPD. The * denotes instances of when the height of the current 100-yr ESL event occurs more often than the present-day frequency of exceeding MHHW (given for each tide gauge in the supporting information). The mapping of tide gauges to cities is given in the supporting information.

					2.0 °C								
		2010 EAE (millions)			2050 EAE AF			2070 EAE AF			2100 EAE AF		
City	Population (millions)	None	1-yr	10-yr	None	1-yr	10-yr	None	1-yr	10-yr	None	1-yr	10-yr
Shenzhen, China	12.52	1.07	0.70	0.70	1.3	2.0	2.0	1.6	2.5	2.5	2.3	3.5	3.5
Vancouver, Canada	1.81	0.20	0.13	0.13	1.0	1.6	1.6	1.0	1.7	1.7	1.1	1.8	1.8
New York, NY, USA	12.52	0.22	0.15	0.15	1.4	2.1	2.1	1.8	2.6	2.6	2.8	4.1	4.1
London, UK	9.88	0.04	0.03	0.03	3.0	3.6	3.6	5.0	5.9	5.9	9.9	11.7	11.6
Buenos Aires, Argentina	11.98	0.03	0.03	0.03	2.0	2.1	2.1	3.4	3.5	3.5	11.7	12.1	12.2
San Diego, CA, USA	2.32	<0.01	<0.01	<0.01	2.4	4.3	4.3	5.2	9.1	9.1	12.5	21.8	21.8
Rio de Janeiro, Brazil	9.11	0.03	0.02	0.02	1.3	2.2	2.2	2.0	3.3	3.3	4.1	6.7	6.7
Hong Kong, China	22.23	3.99	2.53	2.53	1.2	1.9	1.9	1.4	2.2	2.2	2.1	3.3	3.3
Manila, Philippines	5.78	2.06	1.24	1.24	1.1	1.8	1.8	1.1	1.9	1.9	1.3	2.2	2.2
Copenhagen, Denmark	1.34	0.02	0.01	0.01	2.3	3.8	3.8	4.9	7.8	7.8	15.1	24.4	24.4
Dar es Salaam, Tanzania	2.32	0.02	0.01	0.01	1.2	2.3	2.3	2.2	3.9	3.9	3.3	5.9	5.9
Sydney, Australia	3.48	0.01	<0.01	<0.01	1.1	1.8	1.8	1.2	2.0	2.0	3.2	5.2	5.2
Phuket, Thailand	0.16	0.01	0.01	0.01	2.0	2.3	2.3	2.3	3.4	2.3	3.4	3.4	3.4
Tokyo, Japan	25.34	0.55	0.38	0.38	1.4	2.1	2.1	2.0	2.9	2.9	5.9	8.7	8.7
New Orleans, LA, USA	0.71	0.17	0.13	0.13	2.2	3.0	3.0	2.8	3.7	3.7	3.6	4.7	4.7
Norfolk, VA, USA	0.69	<0.01	<0.01	<0.01	2.0	2.7	6.9	3.4	4.7	13.7	13.9	19.0	55.5
San Juan, Puerto Rico	1.82	<0.01	<0.01	<0.01	2.5	2.6	2.7	3.0	3.1	3.3	16.6	17.3	18.3

Table S-4: expected annual population exposure (EAE; millions) under different assumptions of existing coastal flood protection (no protection and protection against the 1-yr and 10-yr events) and amplification factors (AFs) for the EAE for 2050, 2070, and 2100 under the same coastal flood protection assumptions and under a climate scenario in which global mean surface air temperature is stabilized in 2100 at +2 °C (relative to 1850–1900; Bamber et al, 2019).